Inflammation Research (2023) 72:553–576
https://doi.org/10.1007/s00011-022-01653-4

Inflammation Research

ORIGINAL RESEARCH

Human bone marrow mesenchymal stem cell-derived extracellular vesicles reduce inflammation and pyroptosis in acute kidney injury via miR-223-3p/HDAC2/SNRK

Zhijuan Xie[1] · Jun Tang[2] · Zhong Chen[3] · Lanji Wei[4] · Jianying Chen[5] · Qin Liu[1]

Received: 16 June 2022 / Accepted: 23 September 2022 / Published online: 14 January 2023

Abstract

Objective Bone marrow mesenchymal stem cell (BMSC)-derived extracellular vesicles (EVs) have been demonstrated as a potential therapeutic agent in acute kidney injury (AKI). However, little is known about the mechanisms of action of BMSC-derived EVs in AKI. Based on this, our research was designed to investigate the mechanism behind BMSC-derived EVs controlling inflammation and pyroptosis during AKI.

Methods Peripheral blood from AKI patients was used for detection of microRNA (miR)-223-3p, HDAC2, and SNRK expression. An AKI rat model was established, and HK-2 cell injury was induced by lipopolysaccharide (LPS) to establish a cellular model. Co-culture with BMSC-derived EVs and/or gain- and loss-of-function assays were conducted in LPS-treated HK-2 to evaluate the functions of BMSCs-EVs, miR-223-3p, HDAC2, and SNRK. AKI rats were simultaneously injected with EVs and short hairpin RNAs targeting SNRK. The interactions among miR-223-3p, HDAC2, and SNRK were evaluated by RIP, ChIP, and dual-luciferase gene reporter assays.

Results Patients with AKI had low miR-223-3p and SNRK expression and high HDAC2 expression in peripheral blood. Mechanistically, miR-223-3p targeted HDAC2 to accelerate SNRK transcription. In LPS-treated HK-2 cells, BMSCs-EVs overexpressing miR-223-3p increased cell viability and diminished cell apoptosis, KIM-1, LDH, IL-1β, IL-6, TNF-α, NLRP3, ASC, cleaved caspase-1, and IL-18 expression, and GSDMD cleavage, which was nullified by HDAC2 overexpression or SNRK silencing. In AKI rats, BMSCs-EV-shuttled miR-223-3p reduced CRE and BUN levels, apoptosis, inflammation, and pyroptosis, which was abrogated by SNRK silencing.

Conclusion Conclusively, BMSC-derived EV-encapsulated miR-223-3p mitigated AKI-induced inflammation and pyroptosis by targeting HDAC2 and promoting SNRK transcription.

Keywords Acute kidney injury · Bone marrow mesenchymal stem cells · MicroRNA-223-3p · HDAC2 · SNRK · Inflammation · Pyroptosis

Responsible Editor: John Di Battista.

✉ Qin Liu
287814438@qq.com

[1] Department of Nephrology, The First Affiliated Hospital, Hengyang Medical School, University of South China, No. 69 Chuanshan Road, Hengyang 421001, Hunan, People's Republic of China

[2] Department of Emergency, The First Affiliated Hospital, Hengyang Medical School, University of South China, Hengyang 421001, Hunan, People's Republic of China

[3] Department of Nuclear Medicine, The First Affiliated Hospital, Hengyang Medical School, University of South China, Hengyang 421001, Hunan, People's Republic of China

[4] Health Management Center, The Affiliated Nanhua Hospital, Hengyang Medical School, University of South China, Hengyang 421001, Hunan, People's Republic of China

[5] Department of Rheumatology and Immunology, Hunan Province Mawangdui Hospital, Changsha 410016, Hunan, People's Republic of China

Introduction

Acute kidney injury (AKI) is not a single disease entity but a heterogeneous group of diseases accompanied by a sudden reduction in glomerular filtration rate [1]. AKI is characterized by a rapid elevation in serum creatinine, a decline in urine output, or both [2]. AKI can result in deadly complications as fluid and waste accumulate in the body and can even cause death if left untreated [3]. Thus, kidney replacement therapy is usually required, but AKI has a terrible prognosis in critically ill patients [4]. Based on this, the pathophysiological mechanism underpinning AKI still needs to be addressed. AKI has been widely accepted to have relations with intrarenal and systemic inflammation [5]. Pyroptosis is an inflammatory type of programmed cell death, the alteration of which is involved in various autoimmune and auto-inflammatory conditions [6]. Pyroptotic cells secrete proinflammatory factors into the extracellular milieu to trigger inflammation and immune responses [7]. Moreover, pyroptosis is implicated in the maintenance of homeostasis in kidney tissues, thereby orchestrating the pathogenesis of AKI [8]. Exploring molecular mechanisms in inflammation and pyroptosis is vital for the identification of effective therapies to prevent or mitigate AKI.

Bone marrow-derived mesenchymal stem cells (BMSCs), a cell type with the ability of multi-directional differentiation, have been documented to repress pyroptosis of renal tubular epithelial cells in kidney tissues to relieve sepsis-induced AKI [9]. Extracellular vesicles (EVs) are now considered a mechanism for intercellular communication allowing cells to exchange proteins, lipids, DNA, mRNA, and non-coding RNAs [10], which can be released from a number of cell types, like T cells, dendritic cells, B cells, and MSCs [11]. Moreover, it has previously been observed that BMSC-derived EVs could curb renal tubular epithelial cell apoptosis and induce functional recovery and histological protection in ischemia/reperfusion (I/R) injury, the principal cause for AKI, by delivering microRNA (miR)-199a-3p [12]. This finding suggests that miRs play an important role in the action mechanisms of BMSC-derived EVs in AKI.

The role of miRs in AKI is extensively studied, and evidence has revealed that miRs are obviously altered in multiple kinds of AKI [13]. Specifically, an earlier study illustrated that miR-223-3p upregulation suppressed renal tubular epithelial cell pyroptosis to alleviate lipopolysaccharide (LPS)-induced AKI [14]. Also, miR-223-3p overexpression has been shown to lighten calcium oxalate nephrocalcinosis-stimulated kidney inflammation [15]. Moreover, the starBase software used in our study predicted a binding site between miR-223-3p and histone deacetylase 2 (HDAC2). Previous research established that ectopically expressed HDAC2 accelerated renal tubular epithelial cell apoptosis in AKI [16]. Reportedly, HDAC2 controls chromatin structure and transcription by catalyzing deacetylation of histones at the promoter and coding regions of transcribed genes [17]. Additionally, the existence of peak histone H3 acetylation in the sucrose nonfermenting-1 (SNF1)-related kinase (SNRK) promoter region was predicted by the UCSC database in our study. An existing study uncovered that angiotensin II-induced miR-103a-3p upregulation inhibited SNRK expression in glomerular endothelial cells and activated the NF-κB/p65 signaling pathway, thus facilitating renal inflammation and injury [18], which highlighted the significance of SNRK in protection against angiotensin II-induced renal injury. However, the relationship between miR-223-3p and SNRK remains unclear in AKI.

Under this circumstance, we speculated that BMSC-released EVs might carry miR-223-3p to restrain AKI-caused inflammation and pyroptosis via the HDAC2/SNRK axis. This dissertation seeks to verify this speculation and contribute to a deeper understanding of the mechanisms behind AKI.

Materials and methods

Ethics statement

The patients gave their consent to the collection and use of blood and signed an informed consent form. In addition, the experiments involving humans were also ratified by the Ethics Committee of The First Affiliated Hospital, Hengyang Medical School, University of South China, and fully conformed to the *Declaration of Helsinki*. All animal experiments complied with the regulations and codes of practice for the management of laboratory animals, and were reviewed and approved by the Animal Ethics Committee of The First Affiliated Hospital, Hengyang Medical School, University of South China.

Patients and peripheral blood collection

Blood samples were obtained from 20 AKI patients (15 men and 5 women, a mean age of 52–66 years) who visited The First Affiliated Hospital, Hengyang Medical School, University of South China from March 2016 to December 2017, and from 20 healthy individuals who underwent a physical examination at the medical examination center (12 men and 8 women, a mean age of 51–65 years). Venous blood (5 mL) was attained from each participant with a purple blood collection tube containing ethylene diamine tetraacetic acid

anticoagulant and sent to the central laboratory for sample preparation within 3 h.

Cell culture

Human BMSCs (CP-H166) and human renal tubular epithelial cells HK-2 were acquired from Procell (Wuhan, China). BMSC culture was conducted in Dulbecco's Modified Eagle Medium–Low Glucose (DMEM-LG) encompassing 10% fetal bovine serum (FBS; Life Technologies, Grand Island, NY, USA) [19]. HK-2 cell culture was performed in DMEM (Gibco, Grand Island, NY, USA) encompassing 10% FBS. The media were supplemented with 1% penicillin/streptomycin, and all cells were cultured at 37 °C with 5% CO_2.

Identification of BMSCs

The medium for BMSC culture was renewed every 3 days, and BMSCs were collected by multiple times of digestion and passaged when cell confluence reached 80%. Following the collection of the third generation of BMSCs, the expression of surface markers (positive markers included CD44, CD90, and CD29, and negative markers were CD45 and CD34) was detected using a flow cytometer (Beckman, Miami, FL, USA). In addition, the BMSCs were stained for analyses of adipogenic, osteogenic, and chondrogenic differentiation abilities after 14 and 21 days of growth and differentiation using Oil red O solution (ab150678, Abcam, Cambridge, UK), Alizarin Red S (ARS) solution (GP1055, Servicebio, Wuhan, China), and Alcian blue solution (BP-DL241, SenBeiJia Biological Technology Co., Ltd., Nanjing, China), respectively. Subsequent to identification, only the third generation of BMSCs was selected for experimentations.

Extraction and characterization of EVs

Extraction of EVs from BMSCs (BMSCs-EVs) was performed as previously described [20]. Specifically, BMSCs were seeded in 6-well plates containing MSC growth medium at a density of 1×10^5 cells/well for 24-h incubation. After three phosphate-buffered saline (PBS) washes, the BMSCs were cultured in EV-free medium for 48 h. After that, 2 mL of cell culture supernatant were collected and centrifuged (4 °C) at 500 and 2000 g for 15 min each to remove cells, cell debris, or apoptotic bodies. Large vesicles in the supernatant were removed by 20 min centrifugation at 10,000 g. Following centrifugation, the supernatant was collected and retained by filtration through a 0.22 μm filter membrane. EVs were precipitated by 70 min ultracentrifugation at 110,000 g. The precipitate was then resuspended in 1 × PBS and centrifuged at 110,000 g for 70 min to eliminate contaminating proteins. Finally, the precipitate was resuspended in 1 × PBS and preserved at − 80 °C.

EVs were identified by a nanoparticle tracking analysis (NTA) of the particle size on the NanoSight NS300 instrument (Malvern Panalytical, Malvern, UK), observation of morphology using transmission electron microscopy (TEM), and detection of marker protein expression by western blotting. The particle size was analyzed as follows: 10–20 μL of EVs were diluted to 1 mL with PBS, and then, the samples were placed on the NanoSight NS300 and evaluated at a constant flow rate at 25 °C. The morphology of EVs was observed by TEM as follows: 20 μL of EV samples were added dropwise onto a copper grid, placed at room temperature for 2 min, and then negatively stained for 5 min with 3% (w/v) sodium phosphotungstate (12,501-23-4, Sigma-Aldrich, St. Louis, MO, USA). Next, the grid was washed three times with PBS to remove excess sodium phosphotungstate, and then, the EV morphology was observed by TEM (Hitachi H7650, Hitachi, Tokyo, Japan). The experimental methods and specific antibodies for EV marker proteins [CD9, CD63, tumor susceptibility gene 101 (TSG101), and Calnexin] of western blotting were described in the following western blotting section.

Cellular uptake assay of EVs

Cellular uptake of EVs was observed using a PKH26 kit (Sigma-Aldrich). In detail, EVs were resuspended in 1 mL of diluent C, followed by the addition of 4 μL of PKH26 dye for 4 min incubation at room temperature. Then, 2 mL of 1% bovine serum albumin was supplemented and incubated for 1 min at room temperature in the dark to bind to the excess dye and terminate the staining. The labeled EVs were obtained by 70 min centrifugation at 100,000 g and resuspended in PBS. The PKH26-labeled EVs were then co-cultured with HK-2 cells for 12 h. The cells were fixed with 4% paraformaldehyde, rinsed with PBS, and then stained with 4', 6-diamidino-2-phenylindole (DAPI), followed by observation under a laser scanning confocal microscope (Olympus, Tokyo, Japan).

Construction of an AKI cell model

An AKI cell model in HK-2 cells was developed with reference to the description of previous literature [21]. Briefly, the cell culture medium was supplemented with lipopolysaccharide (LPS, 1 μg/mL, Sigma-Aldrich) and then incubated with HK-2 cells for 24 h to induce inflammation before the cells were seeded onto 60 mm culture plates (1×10^6 cells/mL) and incubated for 16 h at 37 °C. Control cells were treated with the same dose of physiological saline.

miR-223-3p overexpression

In the light of the manufacturer's protocols, BMSCs were transduced with miR-223-3p overexpression vector (miR-223-3p agomir; GenePharma, Shanghai, China) or negative control (NC) vector (agomir NC; GenePharma) at a dosage of 20 μL for 48 h, followed by the extraction of EVs (named BMSCs-miR-223-3p-EVs and BMSCs-agomir NC-EVs) for subsequent experiments. miR-223-3p overexpression and NC vectors were transfected into BMSCs only. EVs in the EV co-culture experiments were extracted from the culture supernatant of BMSCs.

Co-culture of BMSCs with HK-2 cells

BMSCs were co-cultured with HK-2 cells in Transwell chambers (Corning Incorporated, Corning, NY, USA) separated by polycarbonate membrane inserts with a well size of 0.4 μm. BMSCs and HK-2 cells were, respectively, seeded in the apical chamber and the basolateral chamber at 2×10^4 cells/well. Following 24 h co-culture, HK-2 cells in the basolateral chamber were obtained for following experimentations. HK-2 cells co-cultured with PBS were used as controls.

To verify whether the functioning components were EVs, an EV inhibition assay was performed. GW4869 (10 μM; Sigma-Aldrich), a neutral sphingomyelinase inhibitor, was used to repress the release of EVs from BMSCs, and BMSCs treated with dimethyl sulfoxide (DMSO) were used as controls. After 12 h, BMSCs were washed three times with sterile PBS and then cultured with 10 mL of serum-free DMEM/F12 (Gibco) for 2 h before co-culture with HK-2 cells.

HK-2 cell transfection and grouping

HK-2 cells were cultured as described above. HDAC2 overexpression vectors (OE-HDAC2), NC overexpression vectors (OE-NC), HDAC2 silencing vectors [short hairpin (sh)-HDAC2], SNRK silencing vectors (sh-SNRK), and NC silencing vectors (sh-NC) were purchased from GenePharma and delivered at a dosage of 50 nM. Subsequent experiments were performed 48 h after transfection. The cells were assigned into control, LPS, LPS + BMSCs, LPS + BMSCs + GM4869, LPS + BMSCs-agomir NC-EVs, LPS + BMSCs-miR-223-3p-EVs, BMSCs-agomir NC-EVs + OE-NC, BMSCs-miR-223-3p-EVs + OE-NC, BMSCs-miR-223-3p-EVs + OE-HDAC2, sh-NC, sh-HDAC2, sh-HDAC2 + DMSO, sh-HDAC2 + ITSA-1 (an activator of HDAC2; 10 μmol/L; 200,626–61-5, MedChem Express, Monmouth Junction, NJ, USA) [22], BMSCs-agomir NC-EVs + sh-NC, BMSCs-miR-223-3p-EVs + sh-NC, and BMSCs-miR-223-3p-EVs + sh-SNRK groups.

Quantitative reverse transcription-polymerase chain reactions (qRT-PCR)

Following the collection of rat kidney tissues and LPS-stimulated cells, total RNA was extracted by the Trizol method, and RNA purity and concentration were detected on a NanoDrop Micro Nucleic Acid Assay Instrument. cDNA was obtained based on the protocols of a reverse transcription kit (Takara, Tokyo, Japan). qRT-PCR was carried out using SYBR Green Mix (Takara) on the Biosystems 7300 real-time PCR system (ABI, Foster City, CA, USA), with three replicates per reaction. Data were analyzed using the $2^{-\Delta\Delta Ct}$ method [23]: ΔΔCt = the experimental group (Ct target gene − Ct internal reference) − the control group (Ct target gene − Ct internal reference). Glyceraldehyde-3-phosphate dehydrogenase (GAPDH) and U6 served as internal references. Primers are detailed in Table 1.

Western blotting

Cells or tissues were lysed on ice with radio-immunoprecipitation assay solution (Beyotime, Shanghai, China) for 15 min and then centrifuged at 13,000 g for 5 min before the measurement of protein concentration using a bicinchoninic

Table 1 Primer sequences

Names	Sequences (5′-3′)
miR-223-3p-F-rno	GCAGTGTTACGCTCCGTGTA
miR-223-3p-R-rno	CATGAGCCACACTTGGGGTA
miR-223-3p-F-hsa	CGCTCCGTGTATTTGACAAGC
miR-223-3p-R-hsa	GTAAGCATGTGCCGCACTTG
HDAC2-F-rno	TCCGGAATGTTGCTCGATGT
HDAC2-R-rno	TTGCATTTGAACACCAGGCG
HDAC2-F-hsa	TATGAAGTCTTGTTTCAGTGGCT
HDAC2-R-hsa	GGCTAAGCTATAGAGGGCAAGG
SNRK-F-rno	CGGCTGAGGAGAAACAGCAAC
SNRK-R-rno	TGCTGGTTCAATGAAGGGGAA
SNRK-F-hsa	CGGCTGAGATATCCATGACGA
SNRK-R-hsa	ACCCGTAAAGACATGCCTGG
GAPDH-F-rno	TCTCTGCTCCTCCCTGTTCT
GAPDH-R-rno	TCCCGTTGATGACCAGCTTC
GAPDH-F-hsa	GGTGAAGGTCGGAGTCAACG
GAPDH-R-hsa	TGAAGGGGTCATTGATGGCAAC
U6-F-rno	CAAATTCGTGAAGCGTT
U6-R-rno	TGGTGTCGTGGAGTCG
U6-F-hsa	CTCGCTTCGGCAGCACA
U6-R-hsa	AACGCTTCACGAATTTGCGT

acid kit (Beyotime). Loading buffer was added to denature the proteins in a boiling water bath for 10 min. The sample volume of each group was calculated according to the protein loading amount. Subsequent to loading, the samples were first electrophoresed at 80 V for 30 min, and then, the electrophoresis was conducted at 120 V for 90 min after bromophenol blue entered the separation gel. The proteins were transferred onto polyvinylidene fluoride membranes at a 250 mA current in an ice bath for 100 min. Washing solution was added to wash the membranes three times (1–2 min for each time). After 2 h blocking, the membranes were probed with anti-HDAC2 (ab32117, 1:1000), anti-kidney injury molecule-1 (KIM-1) (ab78494, 1:1000), anti-H3 (ab1791, 1:100), anti-H3K27ac (ab4729, 1:1000), anti-apoptosis-associated speck-like protein containing a CARD (ASC) (ab180799, 1:1000), anti-Nod-like receptor family pyrin domain containing 3 (NLRP3) (ab263899, 1:1000), anti-interleukin (IL)-18 (ab191152, 1:1000), anti-CD9 (ab223052, 1:1000), anti-CD63 (ab216130, 1:200), anti-TSG101 (ab125011, 1:1000), anti-Calnexin (ab133615, 1:1000), anti-GAPDH (ab8245, 1:1000), anti-β-actin (ab8226, 1:1000) (all from Abcam), anti-cleaved caspase-1 [#4199, 1:1000, Cell Signaling Technology (CST), Beverly, MA, USA], anti-SNRK (PA5-59,897, 1:1000, Thermo Fisher Scientific, Waltham, MA, USA), and anti-gasdermin D (GSDMD; sc-81868, Santa Cruz Biotechnology, Santa Cruz, CA, USA) overnight at 4 °C. The membranes were washed three times with Tris-buffered saline with Tween 20 (TBST) for 10 min each time and probed with a secondary antibody [horseradish peroxidase-tagged goat anti-rabbit immunoglobulin G (IgG); A0208, 1:1000, Beyotime] for 2 h at room temperature. The membranes underwent three TBST washes for 10 min each, followed by dropwise addition of enhanced chemiluminescence solution (P0018FS, Beyotime) and detection on a chemiluminescence imaging system (Bio-Rad, Hercules, CA, USA). Relative protein level was expressed as the grayscale value of the corresponding protein band/that of the GAPDH or β-actin protein band and analyzed using the Quantity One v4.6.2 software. The experiment was repeated three times with the mean value calculated.

3-(4,5-Dimethylthiazol-2-yl)-2,5 diphenyl tetrazolium bromide (MTT) assay

HK-2 cells were seeded on 96-well plates, with three replicates for each sample. Then, 10 μL of MTT solution (M6494, Thermo Fisher Scientific) was added into each well for 2 h incubation. Finally, DMSO (Sigma-Aldrich) was added to terminate the reaction, and the optical density (OD) value at 490 nm was measured using a microplate reader (Model 680; Bio-Rad).

Flow cytometry

Apoptosis in HK-2 cells was determined using an Annexin V-Fluorescein Isothiocyanate (FITC) Apoptosis Detection Kit (Beyotime). Cells were harvested by centrifugation after trypsinization and resuspended in binding buffer, followed by 15 min culture with Annexin V-FITC at room temperature. The apoptosis was measured on a flow cytometer. All experiments were repeated three times.

Immunofluorescence

After routine trypsinization, transfected HK-2 cells were counted and incubated in immunofluorescence chambers at 2×10^5 cells/well. After cell confluence reached 60 – 80%, the cells underwent three PBS rinses for 5 min each time and 15 min fixation with 4% paraformaldehyde. Following three PBS rinses for 5 min each time, the cells were permeabilized with 1% Triton X-100 (diluted in PBS) for 2 min on ice and rinsed with PBS 3 times for 5 min each time. The cells were blocked for 1 h in 5% serum, rinsed three times with PBS for 5 min each time, and probed with primary antibodies against KIM-1 (ab78494, 1:300, Abcam) and NLRP3 (MA5-23,919, 1:100, Thermo Fisher Scientific) prepared with PBS. Afterward, the cells were re-probed with green FITC fluorescence-labeled goat anti-rabbit secondary antibody (ab6717, 1:2000, Abcam) for 1 h at room temperature in the dark. Subsequent to 15 min nuclei staining with DAPI, the cells were observed and photographed using a fluorescence microscope under the same exposure conditions. Each experiment was repeated three times.

Enzyme-linked immunosorbent assay (ELISA)

The levels of proinflammatory factors IL-1β, IL-6, and tumor necrosis factor-α (TNF-α) were detected using the corresponding ELISA kits (R&D Systems, Minneapolis, MN, USA). To be specific, 100 μL of samples or standards were placed in the wells for 90 min incubation in a 37 °C incubator and then incubated for 60 and 30 min with specific antibodies and avidin–biotin–peroxidase complex diluent, respectively. Following 20 – 25 min of incubation with tetramethylbenzidine developer, the OD values were assessed at 450 nm with a microplate reader.

Lactate dehydrogenase (LDH) level determination

LDH levels in HK-2 cells were evaluated using an LDH assay kit (A020-2-2, NanJing JianCheng Bioengineering Institute, Nanjing, China) following the manufacturer's manuals. In detail, HK-2 cells were seeded in a 96-well plate, followed by 5-min centrifugation at 400 g and removal of the supernatant. LDH release reagent was diluted ten times

with 150 μL of PBS and mixed with the cells, followed by 1-h incubation at 37 °C. The mixture was then centrifuged at 400 g for 5 min, and 120 μL of supernatant from each well was added into a new 96-well plate. Each well was supplemented with 60 μL of working solution before 30-min incubation at room temperature in the dark. The OD values at 490 nm were measured using the Model 680 microplate reader (Bio-Rad).

RNA immunoprecipitation (RIP) assay

Cells were washed twice with pre-chilled PBS, centrifuged at 1500 rpm for 5 min, and mixed with an equal volume of RIP lysis buffer. Magnetic beads were resuspended with 100 μL of RIP Wash Buffer and incubated with approximate 5 μg of Argonaute 2 (Ago2) antibody (ab32381, 1:100, Abcam) or IgG antibody (NC) for 30 min at room temperature. The centrifuge tubes were placed on a magnetic stand with the supernatant discarded, and each tube was supplemented with 500 μL of RIP Wash Buffer and shaken with the supernatant removed. This washing procedure was repeated once. Next, each tube was added with 500 μL of RIP Wash Buffer, shaken, and placed on ice. The prepared bead tubes were placed on a magnetic stand, followed by removal of the supernatant. Then, each tube was added with 900 μL of RIP Immunoprecipitation Buffer. The cell lysate was rapidly thawed and centrifuged at 14,000 rpm at 4 °C for 10 min. Then, 100 μL of supernatant was added to the bead–antibody complex for overnight incubation at 4 °C. Following transient centrifugation, the tube was placed on a magnetic stand and the supernatant was discarded. After addition of 500 μL of RIP Wash Buffer and shaking, the tube was positioned on the magnetic stand with the supernatant removed, and washed six times. Each sample was added with 150 μL of Proteinase K Buffer to resuspend the magnetic bead-antibody complex, followed by 30-min incubation at 55 °C. The tube was placed on the magnetic stand before collection of the supernatant. miR-223-3p and HDAC2 expression was detected by qRT-PCR after RNA extraction. Each experiment was repeated three times.

Dual-luciferase reporter gene assay

The binding site of miR-223-3p to HDAC2 was predicted by online software starBase (http://www.starbase.sysu.edu.cn/). Based on the predicted results, wild-type (wt) and mutant (mut) sequences of the binding site (wt-HDAC2 and mut-HDAC2) were designed and synthesized. The wt and mut sequences were separately inserted into the luciferase reporter gene vector (pGL3-Promoter) and then co-transfected with miR-223-3p agomir (30 nM) or agomir NC (30 nM) into HEK293T cells (Shanghai Sixin Biotechnology Co., Ltd., Shanghai, China). Subsequent to transfection, firefly luciferase activity and Renilla luciferase activity were determined, and the ratio of firefly luciferase to Renilla luciferase activity was the relative activity of luciferase, with Renilla luciferase activity as an internal reference. The experiment was repeated three times.

Chromatin immunoprecipitation (ChIP) analysis

ChIP analysis was performed using a ChIP analysis kit (Thermo Fisher Scientific). Chromatin was subjected to cross-linking, isolation, and digestion with micrococcus nuclease to obtain DNA fragments according to the manufacturer's protocols. Antibodies against HDAC2 (#57,156, CST), H3K27ac (#8173, CST), and IgG (ab182931, Abcam) were added to the reaction system for immunoprecipitation. The eluted and purified DNA fragments were detected by PCR with the primers of the SNRK promoter (forward, 5'-TGTGATGCCTTTCCTAAGTCCT-3'; reverse, 5'-CCA ATGGTAAGGCTGGGCTA-3'). IgG served as an NC.

Experimental animal treatment and grouping

Forty 8-week-old healthy male Sprague–Dawley (SD) rats were purchased from Hunan SJA Laboratory Animal Co., Ltd. (Hunan, China). The SD rats were housed in a specific pathogen-free animal room at a room temperature of 21 − 25 °C with a relative humidity of 50 − 65%, a 12:12 h light/dark cycle, and free access to water and food. The rats were placed in sham, AKI, BMSCs-miR-223-3p-EVs + sh-SNRK, and BMSCs-miR-223-3p-EVs + sh-NC groups. Rats in the BMSCs-miR-223-3p-EVs + sh-SNRK and BMSCs-miR-223-3p-EVs + sh-NC groups were co-injected with 100 μg of PBS-suspended BMSCs-miR-223-3p-EVs [24, 25] and 1×10^9 TU of sh- NC or sh-SNRK [26, 27] via tail vein before AKI modeling.

Establishment of an AKI rat model

The AKI rat model was generated reference to the descriptions in previous literature [28]. In brief, after acclimating for 1 week, SD rats were fasted for 12 h, but were allowed to drink freely. The rats were then anesthetized with an intraperitoneal injection of pentobarbital sodium and fixed in the supine position. Subsequent to disinfection, an incision was made along the midline of the abdomen to free the mesentery and cecum. Except for sham-operated rats, the remaining rats were subjected to circular ligation below the ileocecal valve with silk thread and a needle was used to perforate the ligated cecum at the front and end. A little of feces was extruded, and the incision was sutured. Rats in the sham group underwent identical treatment except for cecum ligation and perforation.

Periodic acid Schiff (PAS) staining

Paraffin sections of kidney tissues were routinely dewaxed and hydrated, washed with distilled water for 1 min, and stained with periodic acid solution for 30 min. After being rinsed with distilled water, the sections were stained with Schiff reagent for 30 min in the dark, washed with sodium bisulfite solution for 3 × 2 min, counterstained with hematoxylin for 1 min, and rinsed with tap water for 5 min. The sections were photographed under a light microscope after gradient alcohol dehydration, xylene clearing, and neutral gum mounting.

Hematoxylin–eosin (HE) staining

Kidney tissue sections underwent conventional gradient alcohol dehydration, xylene clearing, and deionized water rinsing. After hematoxylin staining for 3 – 5 min, the sections were rinsed with deionized water, differentiated with 1% hydrochloric alcohol for 20 s, and returned to blue with 1% ammonia for 30 s. Then, the sections were rinsed with deionized water and counterstained with 1% eosin solution for 5 min, followed by rinsing with tap water for 5 min and with deionized water for 1 min. The sections were routinely dehydrated (75%, 90%, 95%, and absolute ethanol for 5 min each), cleared (xylene for 10 min × 2 times), dried, and mounted, followed by microscopic observation and photography.

Masson staining

Paraffin sections of kidney tissues were subjected to routine dewaxing, hydration, and 10-min hematoxylin staining. After 10-s differentiation with 1% hydrochloric alcohol, the sections were rinsed with tap water, returned to blue with Masson solution for 5 min, and washed with distilled water for 1 min. Ponceau fuchsin staining buffer was added for 5 min staining, after which the sections underwent 2 min phosphomolybdic acid washing, 1 min weak acid working solution washing, and 1 min aniline blue counterstaining. Then, the sections were washed with weak acid working solution for 1 min, dehydrated with gradient alcohol, and cleared with xylene before neutral gum mounting and observation and photography under a light microscope. Five unconnected fields of view were randomly selected from each section at 400 × magnification, and the percentage of glomerular collagen fibers was calculated based on the collagen fiber staining area using the Image-Pro Plus 6.0 software. The collagen fibers were stained by aniline blue in blue, and muscle fibers and cytoplasm were stained by Ponceau fuchsin in red.

TdT-mediated dUTP-biotin nick end-labeling (TUNEL) staining

Rat kidney tissues were fixed overnight in 4% paraformaldehyde, paraffin-embedded, and then sliced. Five slices of kidney tissues were dewaxed and hydrated, after which each slice was added with 0.25% Triton X-100 solution for 20-min incubation. Fresh TUNEL reaction solution was added to the slices for 1 h of incubation at 37 °C in the dark. Anti-fade agent containing DAPI was used to block the slices before image capture under a fluorescence microscope.

Kidney function testing

The levels of rat kidney function indicators creatinine (CRE) and blood urea nitrogen (BUN) were measured using an automatic biochemical analyzer. Blood was attained from the eyes of rats and then centrifuged at 1,000 rpm for 10 min to separate serum, followed by the detection of serum CRE and BUN levels on the automatic biochemical analyzer.

Statistical analysis

Data were statistically analyzed using the GraphPad prism7 software, and all data were summarized as mean ± standard deviation. Comparisons between two groups were analyzed using the *t* test, while comparisons among multiple groups were performed using one-way analysis of variance, with Tukey's multiple comparisons test for post hoc multiple comparisons. $P < 0.05$ was considered statistically different.

Results

Identification of BMSCs and BMSCs-EVs

To explore the function of BMSCs-EVs containing miRNAs in AKI, we first identified the purchased BMSCs as well as the extracted BMSCs-EVs. Microscopic observation of morphology showed that the BMSCs were long shuttle or shuttle in shape and arranged in a swirling pattern (Fig. 1A). Flow cytometry detection of surface markers of BMSCs displayed positive expression of CD29, CD90, and CD44 but negative expression of CD45 and CD34 (Fig. 1B). The BMSCs were positive for ARS staining, Oil red O staining, and Alcian blue staining after cultures in osteogenic, adipogenic, and chondrogenic differentiation induction media, respectively (Fig. 1C). The aforementioned results suggested that the BMSCs had high purity and homogeneity and was qualified for subsequent experimentations. Then, the extracted BMSCs-EVs were identified, and the BMSCs-EVs exhibited spherical or oval shapes of uniform size and typical characteristics of BMSCs-EVs under the

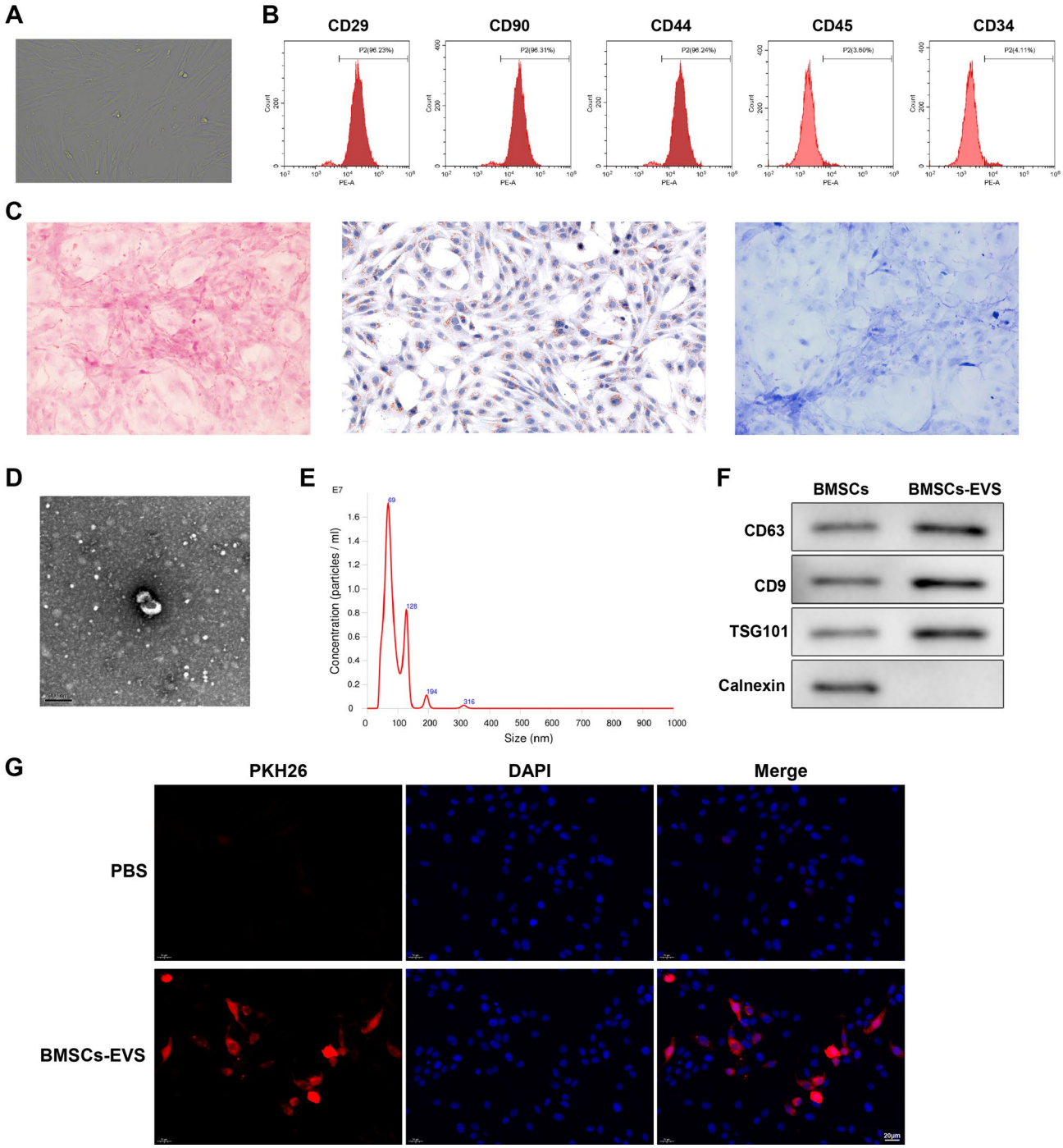

Fig. 1 BMSCs and BMSCs-EVs are identified **A** Morphological observation of BMSCs. **B** Flow cytometry detection of the expression of BMSC markers (CD29, CD44, and CD90) and non-BMSC markers (CD45 and CD34). **C** Identification of osteogenic differentiation (Alizarin Red S staining), adipogenic differentiation (Oil red O staining), and chondrogenic differentiation (Alcian blue staining) of BMSCs. **D** TEM observation of the morphology of BMSCs-EVs' morphology. **E** The nanoparticle tracking analysis of the particle size of BMSCs-EVs. **F** Western blotting detection of CD9, CD63, TSG101, and Calnexin expression in the extracted EVs. **G** Fluorescence microscopy observation of the uptake of PKH26-labeled BMSCs-EVs by HK-2 cells

TEM (Fig. 1D). Moreover, the particle size was within the range of 80–160 nm, shown by the NTA particle-size analysis (Fig. 1E). Immunoblots of EV surface marker proteins depicted that CD9, CD63, and TSG101 were significantly expressed in BMSCs-EVs compared with BMSCs, but Calnexin was not expressed in the EVs (Fig. 1F). Finally, the uptake of PKH26-labeled EVs by LPS-treated HK-2 cells was analyzed, and the fluorescence micrographs showed that a large number of EVs were taken up by LPS-treated HK-2 cells after 12 h of co-culture and were completely distributed around the nucleus, whereas no PKH26 fluorescence was observed in LPS-treated HK-2 cells co-cultured with PBS (Fig. 1G). From the above, EVs were successfully isolated from BM SCs and could be ingested by LPS-treated HK-2 cells.

BMSCs-EVs' attenuated secretion of proinflammatory cytokines and pyroptosis in LPS-treated HK-2 cells

LPS-induced HK-2 cells were co-cultured with BMSCs before and after the addition of GW4869, a specific inhibitor of EV release, to ascertain the impacts of BMSCs-EVs on proinflammatory cytokine release and pyroptosis. Reflected by MTT and flow cytometry results, HK-2 cell viability was obviously decreased and apoptosis rate was substantially increased by LPS treatment ($^{*}P < 0.05$). After co-culture with BMSCs, the viability of LPS-stimulated HK-2 cells was dramatically enhanced and the apoptosis rate was conspicuously diminished (Fig. 2A, B, $^{\#}P < 0.05$). Immunofluorescence and western blotting revealed that KIM-1 (a biomarker of kidney injury) expression in LPS-treated HK-2 cells was signally higher than in control HK-2 cells ($^{*}P < 0.05$). Following co-culture with BMSCs, KIM-1 expression was evidently reduced in the LPS-induced HK-2 cells (Fig. 2C, D, $^{\#}P < 0.05$). The results of ELISA for detecting LDH and proinflammatory factors (IL-1β, IL-6, and TNF-α) showed that LDH, IL-1β, IL-6, and TNF-α levels in the supernatant of HK-2 cells were considerably elevated following LPS treatment ($^{*}P < 0.05$), while co-culture with BMSCs reversed these trends (Fig. 2E, F, $^{\#}P < 0.05$). Immunofluorescence detection of NLRP3 showed that NLRP3 was diffusely distributed in the cytoplasm of control HK-2 cells and gathered in LPS-induced HK-2 cells. The treatment of BMSCs observably diminished NLRP3 spot formation in LPS-treated HK-2 cells (Fig. 2G). Shown by the western blots, LPS-treated HK-2 cells had higher NLRP3, ASC, cleaved caspase-1, and IL-18 protein expression than control HK-2 cells ($^{*}P < 0.05$), whereas these trends were negated by co-culture with BMSCs (Fig. 2H, $^{\#}P < 0.05$). Moreover, GSDMD cleavage and cleaved GSDMD-N were prominently augmented in HK-2 cells by LPS treatment. The co-culture with BMSCs caused a conspicuous decline in GSDMD cleavage and cleaved GSDMD-N in LPS-induced HK-2 cells (Fig. 2I). Interestingly, co-culture of LPS-treated HK-2 cells and GW4869-treated BMSCs strikingly abrogated the attenuating effects of BMSCs on the release of proinflammatory cytokines and pyroptosis in LPS-treated HK-2 cells (Fig. 2A, I and $P < 0.05$). These results indicated that the ameliorative impacts of BMSCs on proinflammatory cytokine secretion and pyroptosis in HK-2 cells were indeed regulated by BMSCs-EVs. Taken together, BMSCs-EVs lightened proinflammatory cytokine release and pyroptosis in LPS-treated HK-2 cells.

BMSCs-EVs overexpressing miR-223-3p repressed proinflammatory cytokine release and pyroptosis in LPS-treated cells

In the above experiments, we noted that BMSCs-EVs relieved proinflammatory cytokine generation and pyroptosis in LPS-treated HK-2 cells, but the related molecular mechanisms remained enigmatic. Therefore, bioinformatics analysis was conducted to predict the potential mechanisms of BMSCs-EVs in AKI. The analysis of the database GSE172039 displayed that miR-223-3p expression was markedly low in the AKI model (Fig. 3A). Therefore, we speculated that BMSCs-EVs lightened proinflammatory cytokine generation and pyroptosis in LPS-treated cells probably by loading miR-223-3p. Subsequently, miR-223-3p expression in AKI patients, LPS-treated HK-2 cells, and BMSCs-EVs was measured by qRT-PCR. The results showed that miR-223-3p was remarkably downregulated in AKI patients or LPS-treated HK-2 cells than in healthy volunteers or control HK-2 cells ($^{*}P < 0.05$) but abundantly expressed in BMSCs-EVs (Fig. 3B, $^{*}P < 0.05$). EVs were extracted from BMSCs after transfection with miR-223-3p agomir or agomir NC. qRT-PCR results manifested that miR-223-3p expression was observably higher in BMSCs-miR-223-3p-EVs than in BMSCs-agomir NC-EVs (Fig. 3C and $P < 0.05$). Then, BMSCs-miR-223-3p-EVs or BMSCs-agomir NC-EVs were co-incubated with LPS-treated HK-2 cells. miR-223-3p expression in LPS-treated HK-2 cells was enhanced in response to the treatment with BMSCs-miR-223-3p-EVs (Fig. 3D and $P < 0.05$). Meanwhile, MTT assay and flow cytometry exhibited that HK-2 cell viability was conspicuously elevated and the apoptosis rate was markedly lowered in the presence of BMSCs-miR-223-3p-EVs (Fig. 3E, F and $P < 0.05$). Shown by immunofluorescence and western blotting, KIM-1 expression in LPS-treated HK-2 cells was substantially diminished by BMSCs-miR-223-3p-EVs (Fig. 3G, H and $P < 0.05$). Moreover, LDH, IL-1β, IL-6, and TNF-α levels were appreciably reduced in the supernatant of LPS-treated HK-2 cells following the treatment with BMSCs-miR-223-3p-EVs (Fig. 3I, J and $P < 0.05$). Immunofluorescence and western blotting

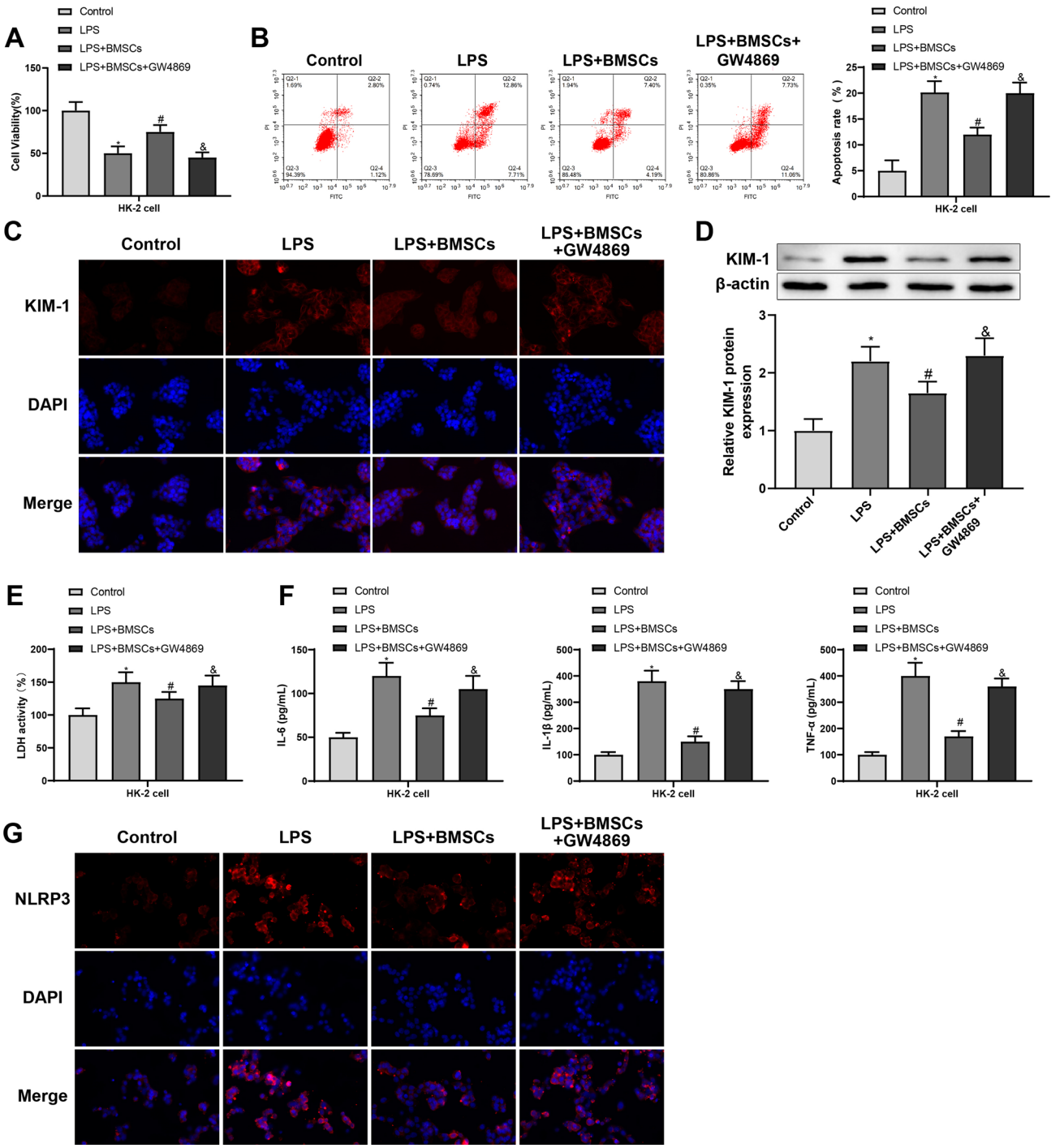

Fig. 2 BMSCs-EVs attenuate proinflammatory cytokine secretion and pyroptosis in LPS-treated cells BMSCs treated with or without GW4869 were co-cultured with LPS-treated HK-2 cells. **A** MTT assay to detect HK-2 cell viability. **B** Flow cytometry to determine HK-2 cell apoptosis. **C**, **D** Immunofluorescence (**C**) and western blotting (**D**) to test the expression of KIM-1. (**E**, **F**) ELISA to analyze changes in the activity of LDH (**E**) and the levels of proinflammatory factors IL-1β, IL-6, and TNF-α (**F**) in supernatants of HK-2 cells. **G** Immunofluorescence to examine NLRP3 expression in HK-2 cells. **H** Western blotting to assess the expression of pyroptosis-related proteins (NLRP3, ASC, cleaved caspase-1, and IL-18) in HK-2 cells. **I** Western blotting detection of GSDMD cleavage in HK-2 cells. Data were expressed as mean ± standard deviation, and each experiment was repeated three times. $^{*}P < 0.05$ vs. control HK-2 cells; $^{\#}P < 0.05$ vs. LPS-induced HK-2 cells; $^{\&}P < 0.05$ vs. LPS-induced HK-2 cells treated with BMSCs

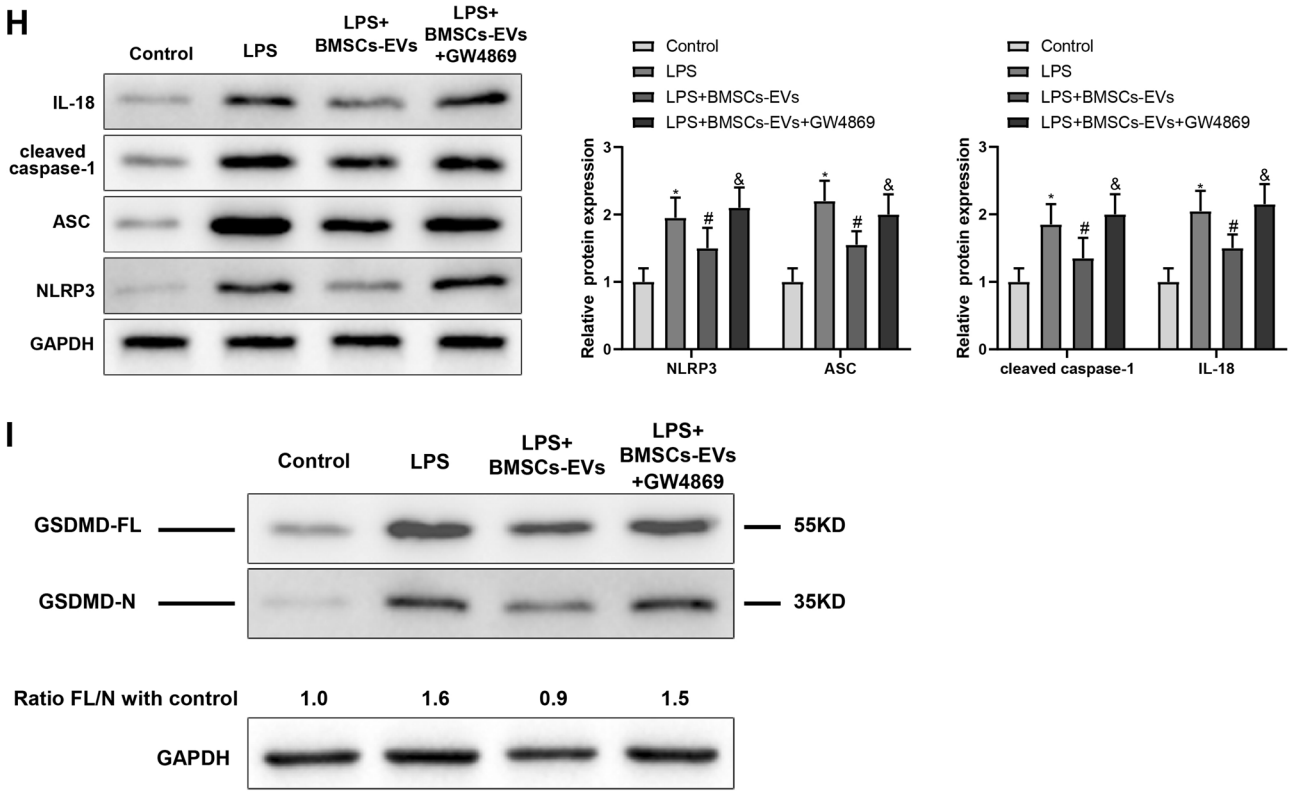

Fig. 2 (continued)

depicted a considerable reduction in NLRP3 spot formation in the cells and decreases in NLRP3, ASC, cleaved caspase-1, and IL-18 protein expression, GSDMD cleavage, and cleaved GSDMD-N in LPS-treated HK-2 cells subsequent to the co-incubation with BMSCs-miR-223-3p-EVs (Fig. 3K, M and $P<0.05$). In summary, overexpression of miR-223-3p in BMSCs-EVs suppressed proinflammatory cytokine production and pyroptosis in LPS-treated HK-2 cells.

BMSCs-EVs carrying miR-223-3p alleviated proinflammatory cytokine production and pyroptosis in LPS-treated HK-2 cells by negatively orchestrating HDAC2 expression

In the aforementioned experiments, we found that BMSCs-EV-packaged miR-223-3p subdued proinflammatory cytokine release and pyroptosis in LPS-treated HK-2 cells, but the related molecular mechanisms were poorly identified. In this context, the molecular mechanism of miR-223-3p in AKI was predicted by bioinformatics analysis. The starBase website predicted that miR-223-3p had a binding site for HDAC2 (Fig. 4A). We, therefore, hypothesized that the repressive influences of BMSCs-EVs overexpressing miR-223-3p on the proinflammatory cytokine secretion and pyroptosis in LPS-treated HK-2 cells might be achieved through HDAC2. HDAC2 expression was first examined in AKI patients and LPS-treated HK-2 cells. Relatedly, HDAC2 mRNA and protein levels were signally increased in the serum of AKI patients as well as in LPS-induced HK-2 cells compared with the controls (Fig. 4B, $^{*}P<0.05$). Next, we explored the relationship between miR-223-3p and HDAC2. RIP assay presented that anti-Ago2 captured a significant amount of HDAC2 mRNA and miR-223-3p versus anti-IgG (Fig. 4C, $^{*}P<0.05$). The results of dual-luciferase reporter gene assay showed that miR-223-3p agomir did not affect the luciferase activity of mut-HDAC2 sequence, but noticeably decreased the luciferase activity of wt-HDAC2 sequence (Fig. 4D, $^{*}P<0.05$). To further investigate the relationship between these two genes, BMSCs-miR-223-3p-EVs or BMSCs-agomir NC-EVs were co-incubated with LPS-stimulated HK-2 cells transfected with OE-HDAC2 or OE-NC. qRT-PCR or western blotting results manifested that HDAC2 mRNA and protein levels in LPS-induced HK-2 cells were dramatically reduced by BMSCs-miR-223-3p-EVs ($^{\#}P<0.05$), which was annulled by OE-HDAC2 transfection (Fig. 4E and $P<0.05$).

Finally, we explored the impacts of co-treatment of BMSCs-miR-223-3p-EVs and OE-HDAC2 on proinflammatory cytokine release and pyroptosis in LPS-treated HK-2

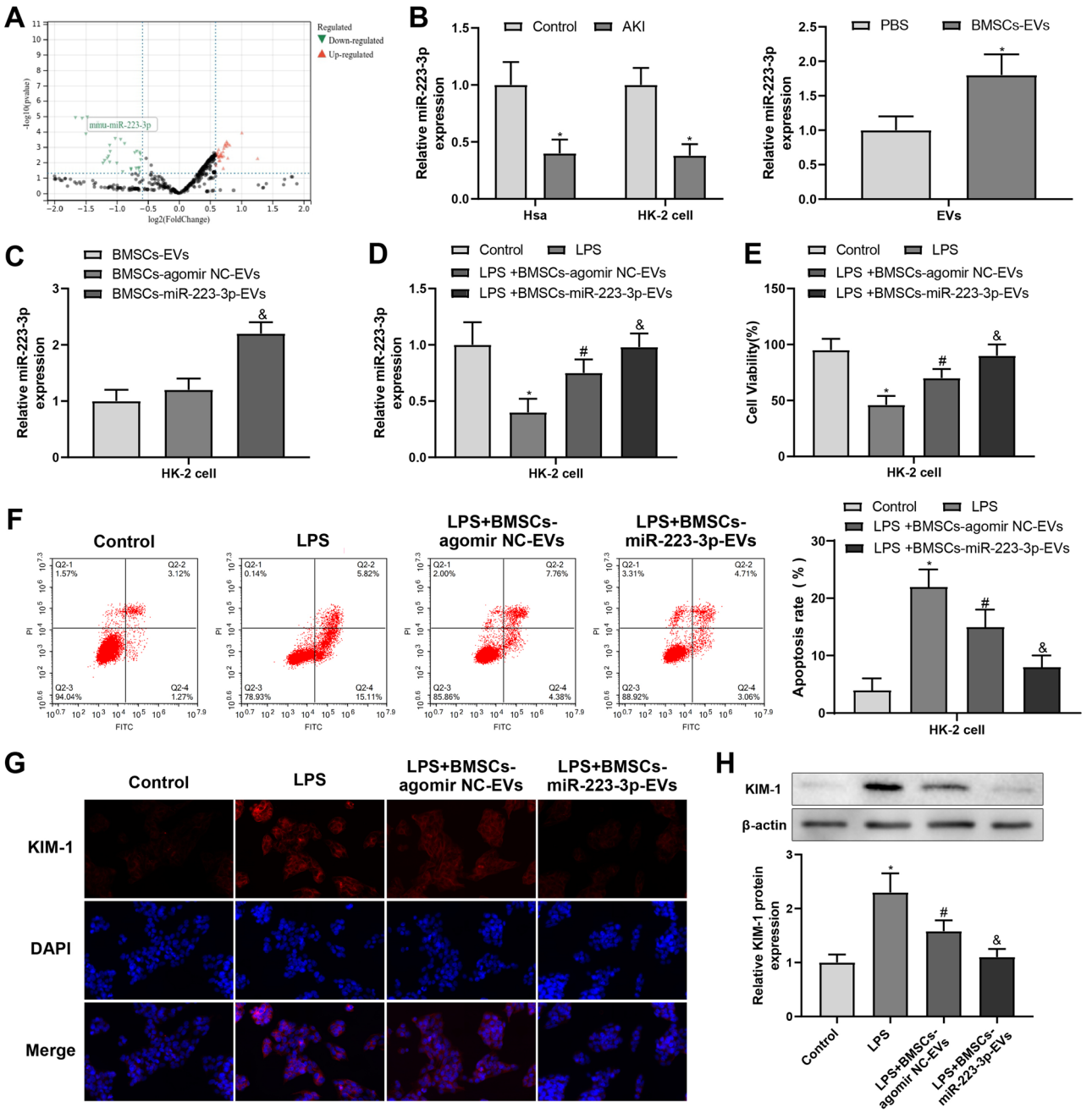
A
Regulated
Down-regulated
Up-regulated
mmu-miR-223-3p
-Log10(pvalue)
log2(FoldChange)
B
Control
AKI
Relative miR-223-3p expression
Hsa
HK-2 cell
PBS
BMSCs-EVs
EVs
C
BMSCs-EVs
BMSCs-agomir NC-EVs
BMSCs-miR-223-3p-EVs
D
Control
LPS
LPS +BMSCs-agomir NC-EVs
LPS +BMSCs-miR-223-3p-EVs
E
Cell Viability(%)
F
Control
LPS
LPS+BMSCs-agomir NC-EVs
LPS+BMSCs-miR-223-3p-EVs
Q2-1 1.57%
Q2-2 3.12%
Q2-3 94.04%
Q2-4 1.27%
Q2-1 0.14%
Q2-2 5.82%
Q2-3 78.93%
Q2-4 15.11%
Q2-1 2.00%
Q2-2 7.76%
Q2-3 85.86%
Q2-4 4.38%
Q2-1 3.31%
Q2-2 4.71%
Q2-3 88.92%
Q2-4 3.06%
PI
FITC
Apoptosis rate (%)
G
KIM-1
DAPI
Merge
H
β-actin
Relative KIM-1 protein expression
I
LDH activity (%)
J
IL-6 (pg/mL)
IL-1β (pg/mL)
TNF-α (pg/mL)

◀ **Fig. 3** BMSCs-EV-delivered miR-223-3p inhibits secretion of proinflammatory cytokines and pyroptosis in LPS-treated HK-2 cells. **A** Analysis of miR-223-3p expression in AKI model of GSE172039 database. **B** qRT-PCR detection of miR-223-3p expression in AKI patients (n=20), LPS-treated HK-2 cells, and BMSCs-EVs. **C** qRT-PCR detection of miR-223-3p in EVs from BMSCs transfected with miR-223-3p agomir. BMSCs-miR-223-3p-EVs or BMSCs-agomir NC-EVs were co-incubated with LPS-treated HK-2 cells. **D** qRT-PCR assay of miR-223-3p expression in HK-2 cells. **E** MTT assay to assess HK-2 cell viability. **F** HK-2 cell apoptosis detected by flow cytometry. **G**, **H** KIM-1 expression in HK-2 cells determined by immunofluorescence (**G**) and western blotting (**H**). **I**, **J** ELISA to measure changes in the expression of LDH (**I**) and proinflammatory factors IL-1β, IL-6, and TNF-α (**J**) in supernatants of HK-2 cells. **K** Immunofluorescence measurement of NLRP3 expression in HK-2 cells. **L** Western blotting analysis of NLRP3, ASC, cleaved caspase-1, and IL-18 protein expression in HK-2 cells; **M** Western blotting to detect GSDMD cleavage in HK-2 cells. Data were expressed as mean±standard deviation, and each experiment was repeated three times. $^{*}P<0.05$ vs. healthy controls or control HK-2 cells; $^{\#}P<0.05$ vs. LPS-treated HK-2 cells; $^{\&}P<0.05$ vs. BMSCs-agomir NC-EVs or LPS-treated HK-2 cells co-incubated with BMSCs-agomir NC-EVs

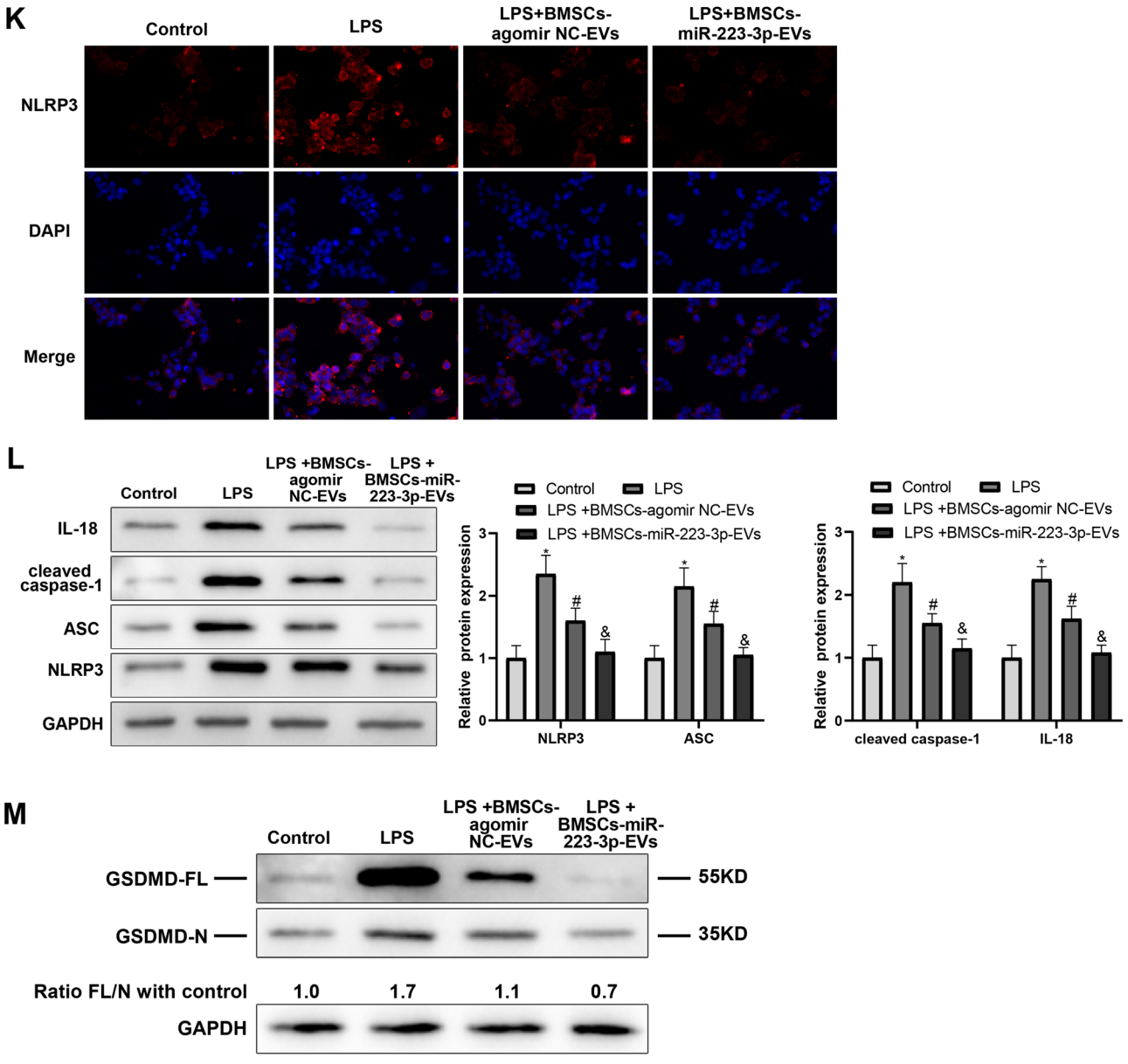

Fig. 3 (continued)

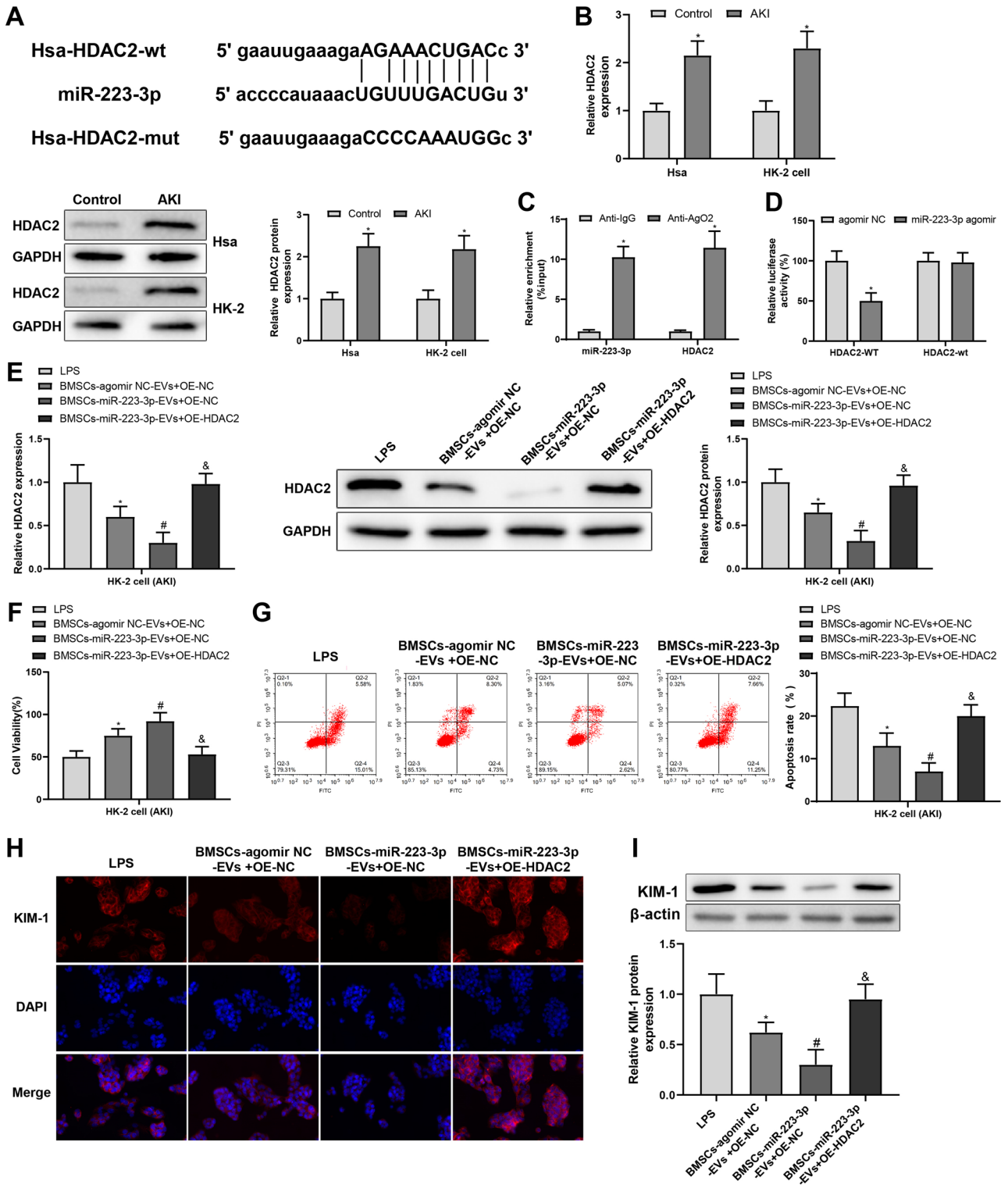
A
Hsa-HDAC2-wt 5' gaauugaaagaAGAAACUGACc 3'
miR-223-3p 5' accccauaaacUGUUUGACUGu 3'
Hsa-HDAC2-mut 5' gaauugaaagaCCCCAAAUGGc 3'
B
Control
AKI
Relative HDAC2 expression
Hsa
HK-2 cell
Control
AKI
HDAC2
GAPDH
Hsa
HDAC2
GAPDH
HK-2
Relative HDAC2 protein expression
C
Anti-IgG
Anti-AgO2
Relative enrichment (%input)
miR-223-3p
HDAC2
D
agomir NC
miR-223-3p agomir
Relative luciferase activity (%)
HDAC2-WT
HDAC2-wt
E
LPS
BMSCs-agomir NC-EVs+OE-NC
BMSCs-miR-223-3p-EVs+OE-NC
BMSCs-miR-223-3p-EVs+OE-HDAC2
Relative HDAC2 expression
HK-2 cell (AKI)
LPS
BMSCs-agomir NC -EVs +OE-NC
BMSCs-miR-223-3p -EVs+OE-NC
BMSCs-miR-223-3p -EVs+OE-HDAC2
HDAC2
GAPDH
Relative HDAC2 protein expression
F
Cell Viability(%)
G
Apoptosis rate (%)
H
KIM-1
DAPI
Merge
I
KIM-1
β-actin
Relative KIM-1 protein expression

◀ **Fig. 4** BMSCs-EV-encapsulated miR-223-3p decreased HDAC2 expression to mitigate release of proinflammatory cytokines and pyroptosis in LPS-treated HK-2 cells Note: **A** The binding site of miR-223-3p to HDAC2 and mutant sequence. **B** HDAC2 mRNA and protein levels in AKI patients ($n=20$) and LPS-treated HK-2 cells detected by qRT-PCR and western blotting. **C**, **D** RIP and dual-luciferase reporter gene assays to verify the binding between miR-223-3p and HDAC2. BMSCs-miR-223-3p-EVs or BMSCs-agomir NC-EVs were co-incubated with LPS-stimulated HK-2 cells transfected with OE-HDAC2 or OE-NC. **E** qRT-PCR and western blotting to measure HDAC2 mRNA and protein levels. **F** MTT assay of cell viability. **G** Apoptosis determined by flow cytometry. **H**, **I** Immunofluorescence (**H**) and western blotting (**I**) analyses of KIM-1 expression. **J**, **K** ELISA analysis of changes in the expression of LDH (**J**) and proinflammatory factors IL-1β, IL-6, and TNF-α (**K**) in cell supernatants. **L** Immunofluorescence assessment of the expression of NLRP3 in HK-2 cells. **M** Western blotting to evaluate the expression of NLRP3, ASC, cleaved caspase-1, and IL-18 proteins. (N) GSDMD cleavage tested by western blotting. Data were expressed as mean ± standard deviation, and each experiment was repeated three times. $^{*}P<0.05$ vs. healthy controls, control HK-2 cells, LPS-treated HK-2 cells, IgG, or agomir NC treatment; $^{\#}P<0.05$ vs. LPS-stimulated HK-2 cells treated with BMSCs-agomir NC-EVs + OE-NC; $^{\&}P<0.05$ vs. LPS-stimulated HK-2 cells treated with BMSCs-miR-223-3p-EVs + OE-NC

cells. MTT and flow cytometry results showed observably reduced viability and conspicuously augmented apoptosis in LPS-treated HK-2 cells co-incubated with BMSCs-miR-223-3p-EVs after the HK-2 cells were transfected with OE-HDAC2 (Fig. 4F, G and $P<0.05$). Moreover, it was observed in the results of immunofluorescence and western blotting that OE-HDAC2 treatment triggered a significant enhancement of KIM-1 expression in LPS-treated HK-2 cells in the presence of BMSCs-miR-223-3p-EVs (Fig. 4H, I and $P<0.05$). Meanwhile, in the presence of BMSCs-miR-223-3p-EVs, HDAC2 overexpression remarkably increased LDH, IL-1β, IL-6, and TNF-α levels in the supernatant of LPS-treated HK-2 cells (Fig. 4J, K and $P<0.05$). Reflected by immunofluorescence and western blotting, an obvious augmentation of NLRP3 spot formation in the cells and increases in NLRP3, ASC, cleaved caspase-1, IL-18, and cleaved GSDMD-N expression were found in LPS-treated HK-2 cells co-incubated with BMSCs-miR-223-3p-EVs in the presence of OE-HDAC2 (Fig. 4L, N and $P<0.05$). In conclusion, BMSCs-EV-encapsulated miR-223-3p curtailed proinflammatory cytokine secretion and pyroptosis in LPS-treated HK-2 cells by downregulating HDAC2.

HDAC2 reduced H3 acetylation level to constrain SNRK transcription

HDAC2 is a histone deacetylase that can reduce H3 acetylation level and thus manipulate downstream target genes. UCSC database analysis revealed the presence of peak H3 acetylation in the promoter region of SNRK (Fig. 5A), suggesting that SNRK transcription was controlled by histone acetylation. Thus, a hypothesis was drawn that SNRK might be involved in the alleviatory effects of miR-223-3p/HDAC2 on proinflammatory cytokine upregulation and pyroptosis in LPS-treated HK-2 cells. First, we examined SNRK expression in AKI patients and HK-2 cells. qRT-PCR and western blotting revealed that SNRK mRNA and protein levels were conspicuously lower in AKI patients and LPS-stimulated HK-2 cells than in the controls (Fig. 5B, $^{*}P<0.05$). A noticeable decline of HDAC2 expression and a prominent elevation of SNRK expression were detected in HK-2 cells following sh-HDAC2 transfection (Fig. 5C, $^{*}P<0.05$), suggesting that HDAC2 may inversely modulate SNRK expression.

Then, we explored whether SNRK expression is directly controlled by HDAC2. ChIP assay depicted that HDAC2 bound to strikingly more SNRK promoter than IgG (Fig. 5D, $^{*}P<0.05$), illustrating that HDAC2 was enriched in the transcriptional regulatory region of SNRK gene. Afterward, we delved into the question whether H3K27ac is implicated in the transcriptional mediation of SNRK by HDAC2. Immunoblots showed no obvious change in total H3 expression but a significant decline of H3K27ac expression in LPS-treated HK-2cells ($^{*}P<0.05$). In response to sh-HDAC2 transfection, total H3 expression was not prominently changed, but H3K27ac expression was substantially augmented in LPS-treated HK-2 cells (Fig. 5E, F, $^{\#}P<0.05$). ChIP assay results demonstrated that the SNRK promoter was precipitated by H3K27ac rather than IgG (Fig. 5G, $^{*}P<0.05$). Transfection with sh-HDAC2 contributed to the enrichment of H3K27ac in the SNRK promoter region (Fig. 5H, $^{\#}P<0.05$). Finally, an HDAC activator ITSA-1 was used to treat HK-2 cells in the presence of sh-HDAC2. As manifested in Fig. 5I, ITSA-1 nullified the promoting impacts of sh-HDAC2 on H3K27ac and SNRK protein expression ($P<0.05$). Collectively, HDAC2 suppressed SNRK transcription by diminishing H3 acetylation in LPS-treated HK-2 cells.

Downregulation of SNRK counteracted the mitigating influences of miR-223-3p-overexpressing BMSCs-EVs on release of proinflammatory cytokines and pyroptosis in LPS-treated HK-2 cells

To clarify whether SNRK participates in the inhibitory impacts of miR-223-3p/HDAC2 on proinflammatory cytokine upregulation and pyroptosis in LPS-treated HK-2 cells, BMSCs-miR-223-3p-EVs or BMSCs-agomir NC-EVs were co-incubated with LPS-stimulated HK-2 cells transfected with sh-SNRK or sh-NC. The results of qRT-PCR or western blotting in Fig. 6A revealed that the treatment of BMSCs-miR-223-3p-EVs noticeably enhanced miR-223-3p and SNRK expression in LPS-stimulated HK-2 cells ($^{\#}P<0.05$). However, sh-SNRK did not markedly affect miR-223-3p expression but noticeably

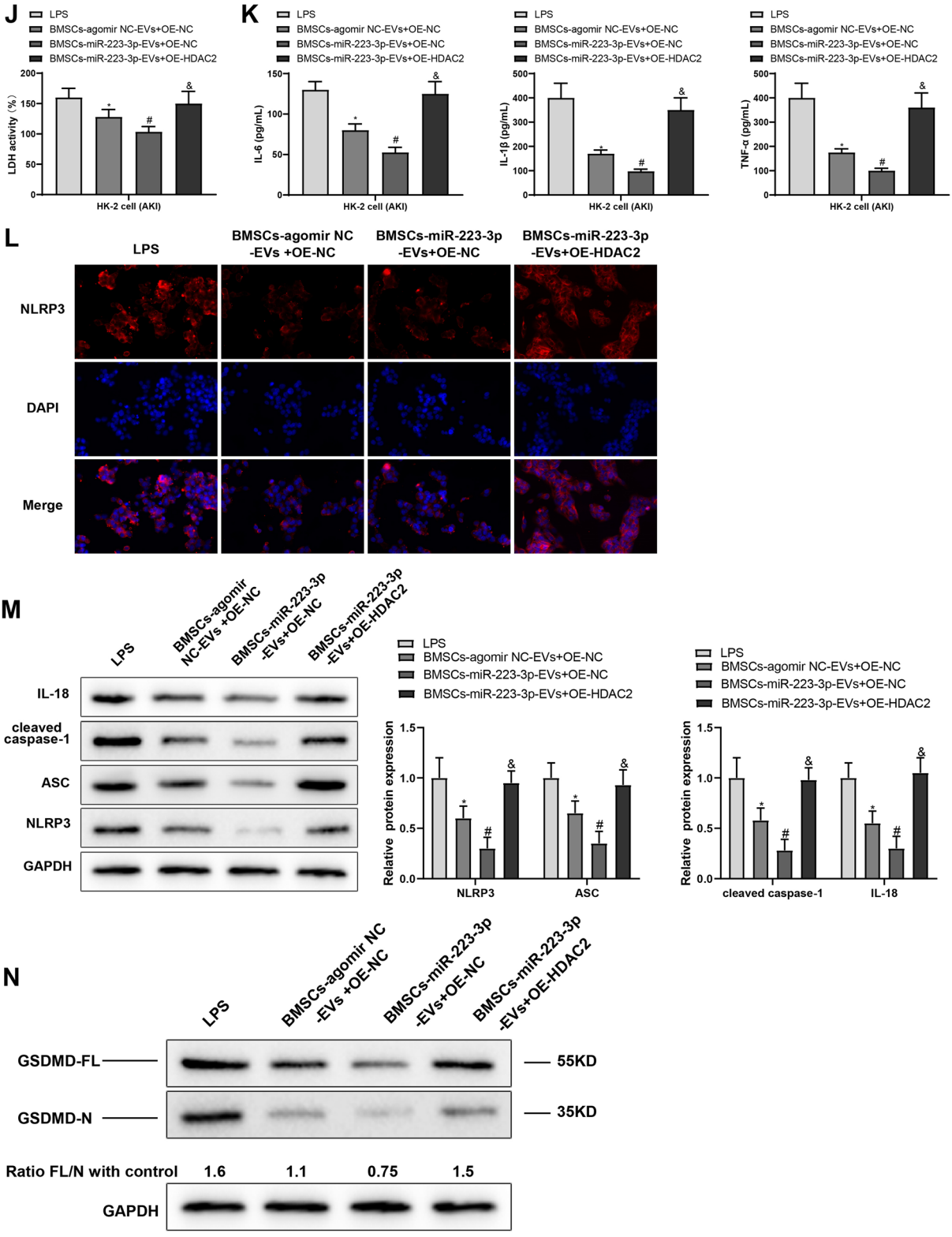

Fig. 4 (continued)

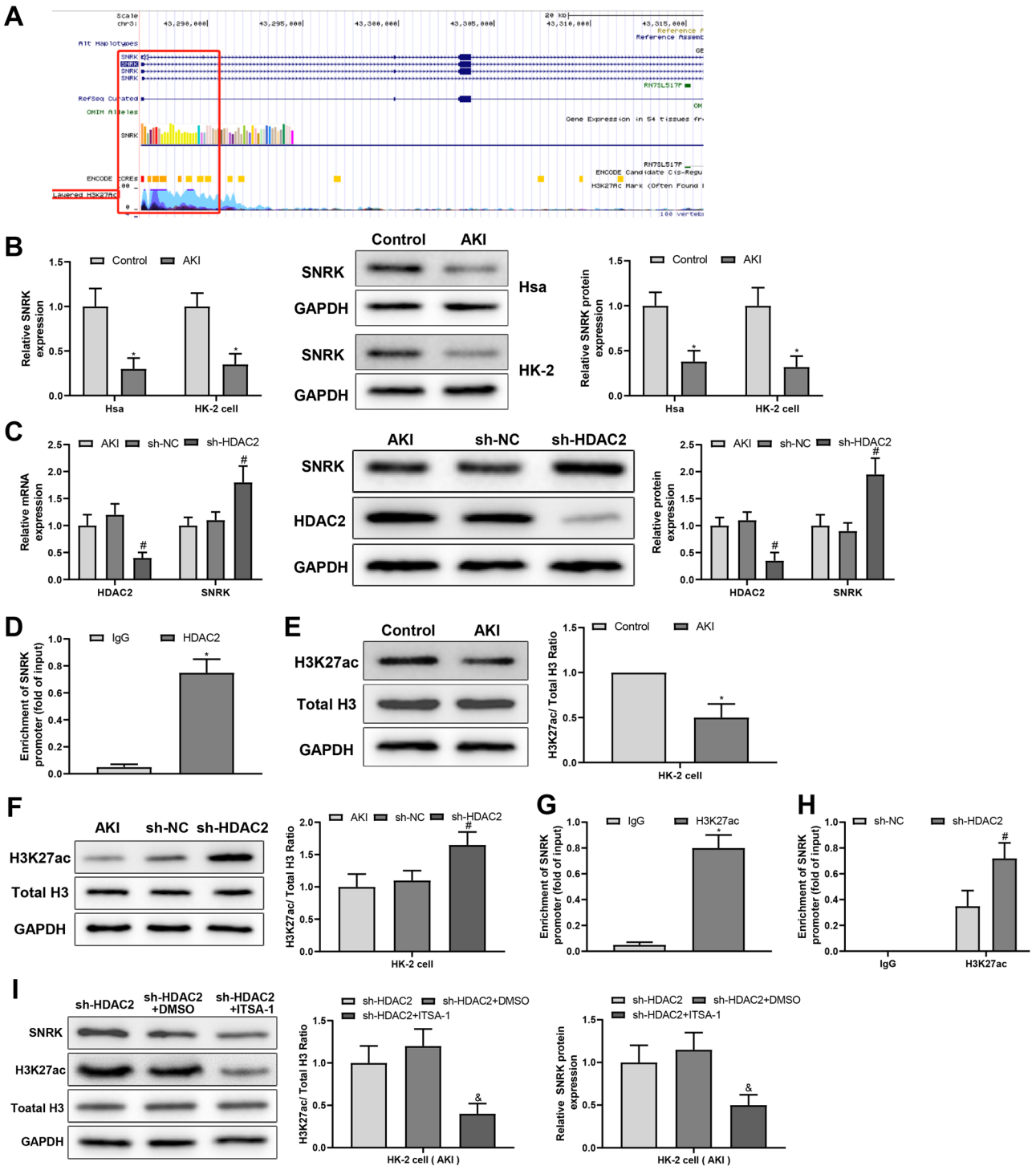

Fig. 5 HDAC2 inhibits H3 acetylation, thus diminishing SNRK transcription **A** UCSC database analysis of histone H3 acetylation in the promoter region of SNRK. **B** qRT-PCR and western blotting detection of SNRK mRNA and protein levels in AKI patients ($n=20$) and LPS-induced HK-2 cells. **C** qRT-PCR and western blotting to determine HDAC2 and SNAK mRNA and protein levels in HK-2 cells transfected with sh-HDAC2. **D** ChIP assay to assess HDAC2 enrichment in the SNRK promoter region. **E**, **F** Western blotting to measure H3K27ac expression in LPS-stimulated HK-2 cells before and after transfection with sh-HDAC2. **G** H3K27ac expression in the SNRK promoter region evaluated by ChIP assay. **H** The enrichment of H3K27ac in the SNRK promoter region in HK-2 cells after transfection with sh-HDAC2 tested by ChIP assay. **I** The expression of H3K27ac, SNRK, and H3 proteins in LPS-stimulated HK-2 cells after the combination treatment of an HDAC activator ITSA-1 (10 μmol/L) and sh-HDAC2 examined by western blotting. Data were expressed as mean ± standard deviation, and each experiment was repeated three times. $^{*}P<0.05$ vs. healthy controls or IgG; $^{\#}P<0.05$ vs. LPS-stimulated HK-2 cells transfected with sh-NC; $^{\&}P<0.05$ vs. LPS-stimulated HK-2 cells treated with sh-HDAC2 + DMSO

reduced SNRK expression in LPS-stimulated HK-2 cells in the presence of BMSCs-miR-223-3p-EVs (Fig. 6A and $P < 0.05$). MTT assay and flow cytometry results exhibited significantly reduced viability and considerably accelerated cell apoptosis in LPS-stimulated HK-2 cells co-incubated with BMSCs-miR-223-3p-EVs after silencing of SNRK (Fig. 6B, C and $P < 0.05$). Depicted by immunofluorescence and western blotting, LPS-stimulated HK-2 cells had observably increased KIM-1 expression after SNRK silencing in the presence of BMSCs-miR-223-3p-EVs (Fig. 6D, E and $P < 0.05$). Moreover, in the supernatant of LPS-stimulated HK-2 cells co-incubated with BMSCs-miR-223-3p-EVs, LDH, IL-1β, IL-6, and TNF-α levels were remarkably elevated in response to sh-SNRK (Fig. 6F, G and $P < 0.05$). Immunofluorescence and western blotting results demonstrated that SNRK silencing substantially increased NLRP3 spot formation in the cells and promoted NLRP3, ASC, cleaved caspase-1, IL-18, and GSDMD-N expression in LPS-stimulated HK-2 cells in the presence of BMSCs-miR-223-3p-EVs (Fig. 6H, J and $P < 0.05$). The above results suggested that SNRK silencing neutralized the attenuating effects of BMSCs-EV-shuttled miR-223-3p on proinflammatory cytokine release and pyroptosis in LPS-treated HK-2 cells.

SNRK silencing abolished the repressive effects of miR-223-3p overexpression in BMSCs-EVs on inflammation and pyroptosis in AKI rats

To further clarify the molecular mechanism of the mitigating influences of BMSCs-EV-packaged miR-223-3p on inflammation and pyroptosis in vivo, AKI rats were injected with BMSCs-miR-223-3p-EVs together with sh-SNRK or sh-NC via tail vein. Demonstrated by qRT-PCR or western blotting, miR-223-3p and SNRK expression was significantly poorer in the kidney tissues of AKI rats than in sham-operated rats ($^{*}P < 0.05$). After the injection of BMSCs-miR-223-3p-EVs alone, the kidney tissues of AKI rats displayed a substantial elevation of miR-223-3p and SNRK expression ($^{\#}P < 0.05$). In the presence of BMSCs-miR-223-3p-EVs, miR-223-3p expression was insignificantly changed and SNRK expression was dramatically decreased by sh-SNRK (Fig. 7A and $P < 0.05$). HE and PAS staining showed that in comparison to sham-operated rats, the glomerular volume of AKI rats considerably increased, and some tubular epithelial cells were vacuolated and degenerated, accompanied by marked deposits of purple–red glycogen and a small amount of inflammatory cell infiltration in the glomerular mesangium. BMSCs-miR-223-3p-EVs culminated in the prominent diminishment of histopathological changes in kidney tissues of AKI rats, which was negated by co-treatment with sh-SNRK (Fig. 7B). TUNEL and Masson staining manifested an increased percentage of TUNEL-positive cells, thickening of glomerular basement membrane, and increased blue staining of renal interstitial collagen fibers in the kidney tissues of AKI rats compared to those in sham-operated rats. The injection of BMSCs-miR-223-3p-EVs observably improved histopathological changes of kidney tissues in AKI rats, whereas SNRK silencing abrogated these trends (Fig. 7B). In addition, the serum levels of CRE and BUN were noticeably increased in rats after AKI modeling ($^{*}P < 0.05$). AKI rats injected with BMSCs-miR-223-3p-EVs exhibited a remarkable decline of CRE and BUN serum levels ($^{\#}P < 0.05$), which was nullified by additional sh-SNRK treatment (Fig. 7C, D and $P < 0.05$). As depicted in the results of ELISA or western blotting, the kidney tissues of rats manifested appreciable increases in IL-1β, IL-6, and TNF-α levels and NLRP3, ASC, cleaved caspase-1, and IL-18 protein expression after AKI modeling ($^{*}P < 0.05$). IL-1β, IL-6, and TNF-α levels as well as NLRP3, ASC, cleaved caspase-1, and IL-18 protein expression in kidney tissues were markedly diminished in AKI rats after the injection of BMSCs-miR-223-3p-EVs ($^{\#}P < 0.05$), which was nullified by additional SNRK silencing (Fig. 7E, F and $P < 0.05$). The aforesaid data indicated that downregulation of SNRK blocked the relieving effects of BMSCs-EV-shuttled miR-223-3p on inflammation and pyroptosis in AKI rats.

Discussion

AKI is a frequent syndrome that not only leads to waste retention, impaired electrolyte balance, and altered drug concentrations but also induces a universal inflammatory response that afflicts distant organs [29]. MSC-EVs have been extensively recognized as a potential cure for AKI, with favorable effectiveness and safety [30]. To broaden the understanding of the mechanisms of MSC-secreted EVs in mitigating AKI, the present study specifically focused on the mechanism by which BMSC-derived EVs repressed inflammation and pyroptosis in AKI. The obtained data provided a notion that BMSC-derived EV-encapsulated miR-223-3p attenuated AKI-induced inflammation and pyroptosis by targeting HDAC2 and facilitating SNRK transcription.

BMSCs have displayed a promise for alleviating AKI through kidney repair [31]. It was evidenced in prior research that BMSCs could curtail I/R injury-induced AKI in rats by releasing tumor necrosis factor-inducible gene 6 protein [32]. Besides the release of soluble molecules, the secretion of EVs is an alternative mechanism of MSCs [33]. BMSC-derived EVs constrained inflammation and cell apoptosis and thereby ameliorated renal I/R injury in rats [34]. The research of Lin et al. uncovered that BMSC-released

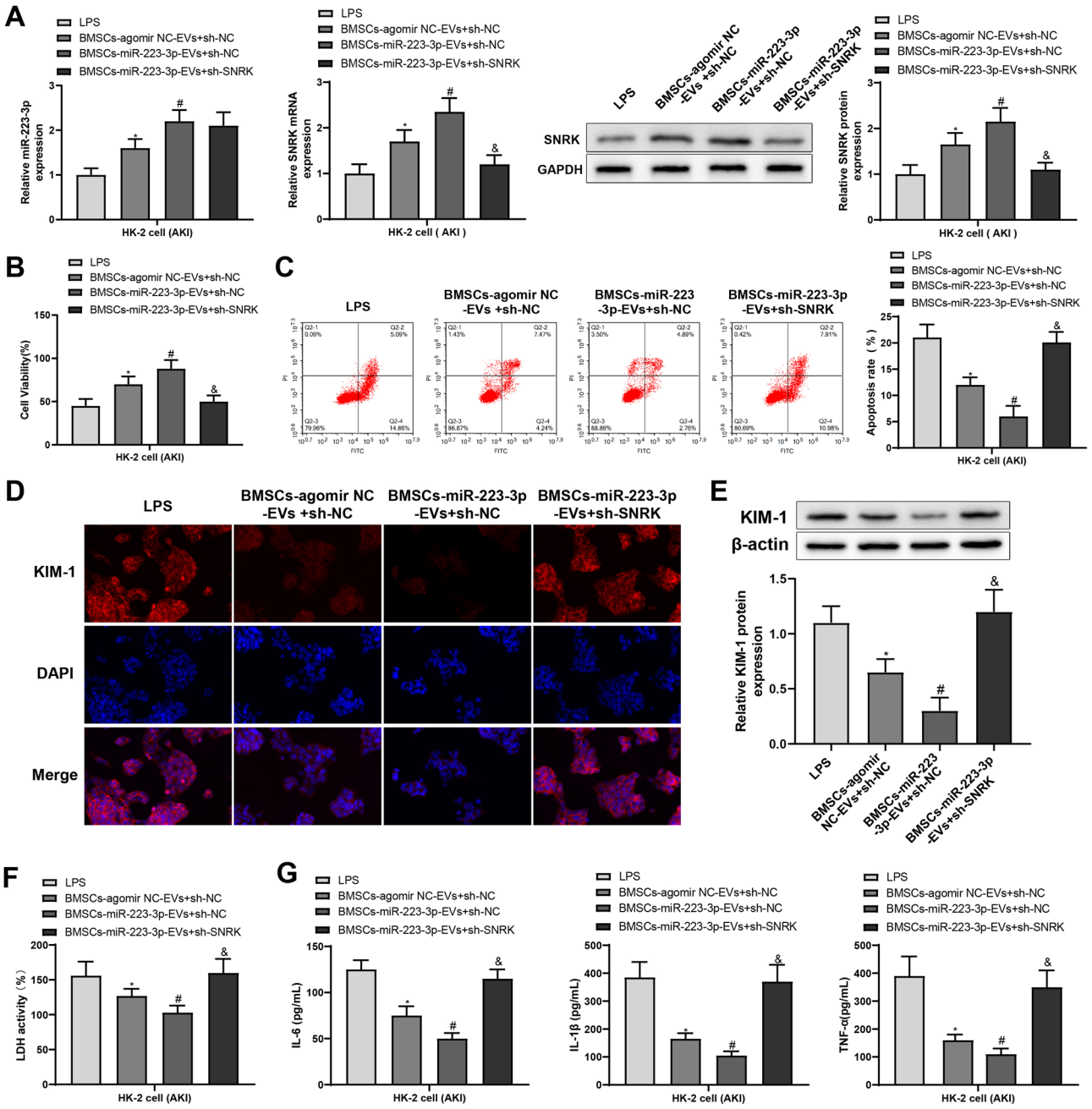

Fig. 6 SNRK silencing counterweighs the inhibitory effects of miR-223-3p upregulation in BMSCs-EVs on secretion of proinflammatory cytokines and pyroptosis in LPS-treated HK-2 cells BMSCs-miR-223-3p-EVs or BMSCs-agomir NC-EVs were co-cultured with LPS-induced HK-2 cells transfected with sh-SNRK or sh-NC. **A** miR-223-3p expression detected by qRT-PCR and SNRK expression measured by qRT-PCR and western blotting in HK-2 cells. **B** MTT assay to detect cell viability. **C** Cell apoptosis assessed by flow cytometry. **D**, **E** Immunofluorescence (**D**) and western blotting (**E**) analyses of KIM-1 expression. **F**, **G** ELISA to detect changes in the expression of LDH (**F**) as well as proinflammatory factors IL-1β, IL-6, and TNF-α (**G**) in cell supernatants. **H** Immunofluorescence detection of NLRP3 expression in cells. **I** NLRP3, ASC, cleaved caspase-1, and IL-18 protein expression tested by western blotting. **J** Immunostaining examination of GSDMD cleavage. Data were expressed as mean ± standard deviation, and each experiment was repeated three times. $^{*}P < 0.05$ vs. LPS-induced HK-2 cells; $^{\#}P < 0.05$ vs. LPS-induced HK-2 cells treated with BMSCs-agomir NC-EVs + sh-NC; $^{\&}P < 0.05$ vs. LPS-induced HK-2 cells treated with BMSCs-miR-223-3p-EVs + sh-NC

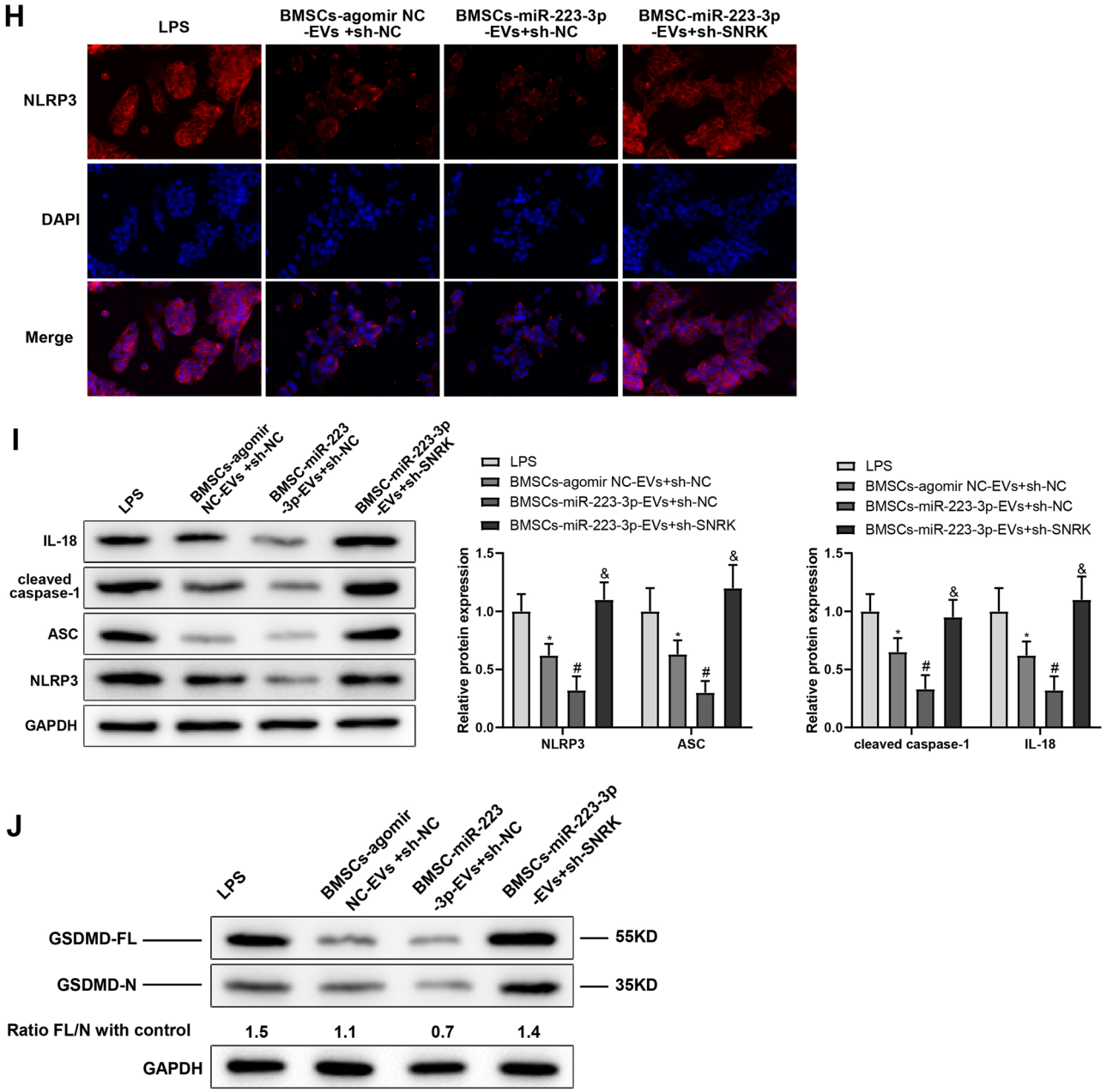

Fig. 6 (continued)

microvesicles also restricted inflammation and pyroptosis of macrophages in atherosclerotic plaques of mice [35]. Corroborating findings were reported in our research that BMSC-secreted EVs subdued apoptosis, proinflammatory cytokine release, and pyroptosis in LPS-treated HK-2 cells, evidenced by reduced IL-1β, IL-6, TNF-α, NLRP3, ASC, cleaved caspase-1, and IL-18 expression, NLRP3 spot formation, and GSDMD cleavage. Meanwhile, our data indicated that co-culture with BMSCs-EVs lowered KIM-1 expression and augmented viability of LPS-treated HK-2 cells. As reported, KIM-1, a biomarker of kidney injury, is poorly expressed in normal kidneys and other organs, but obviously overexpressed after AKI [36]. Taken together, BMSC-derived EVs reduced proinflammatory cytokine secretion and pyroptosis, thus alleviating AKI. A previous study demonstrated that BMSCs minimized Gentamicin-induced AKI in rats potentially via exosome-like microvesicle-carried RNA [25]. Therefore, the alleviatory mechanism of BMSC-EVs in AKI is eminently worth further investigation.

Cells can selectively sort miRNA into EVs for delivery to nearby or distant targets [37]. For instance, BMSC-derived

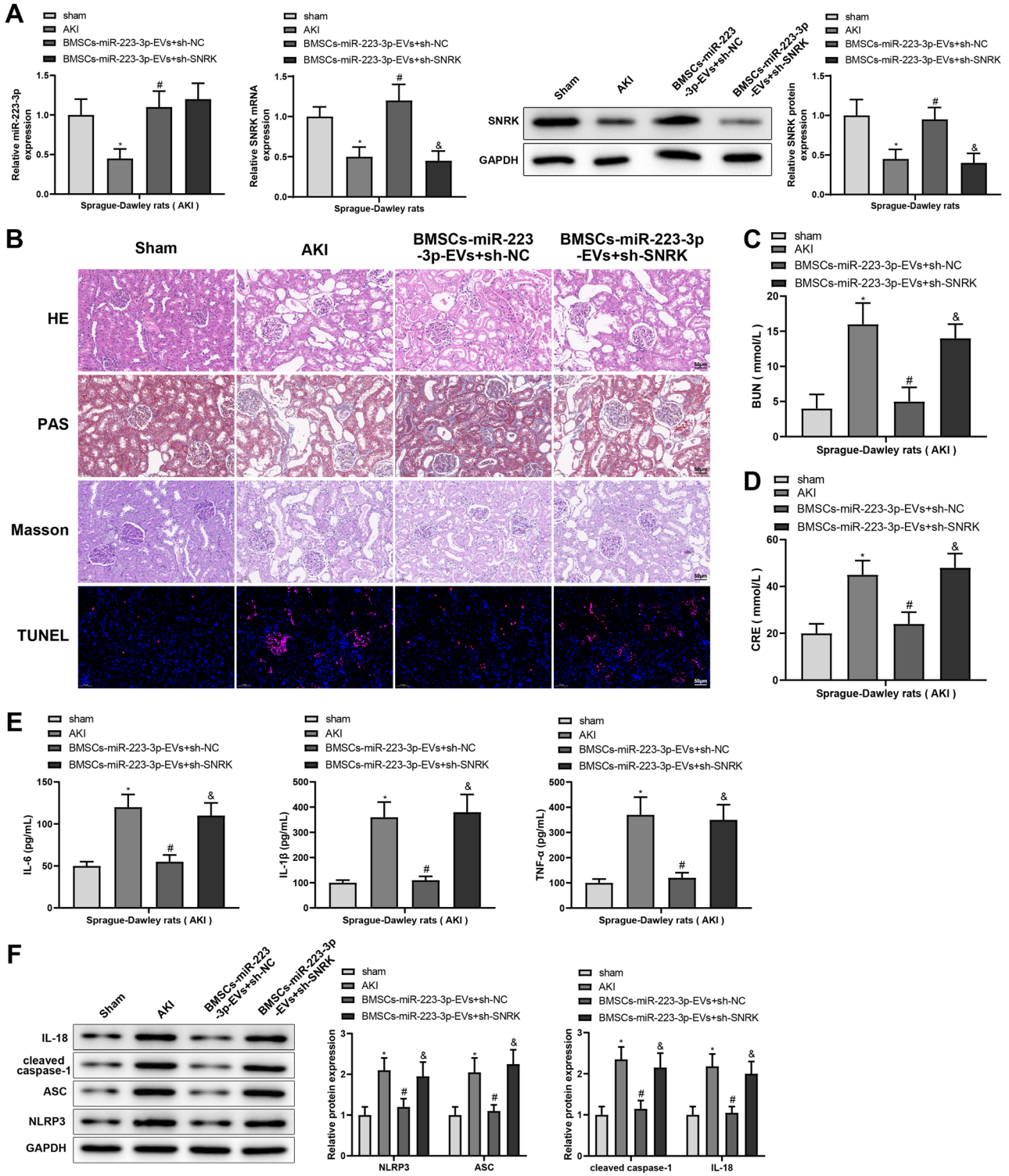

Fig. 7 Downregulation of SNRK nullifies the alleviatory influences of BMSCs-EV-encapsulated miR-223-3p on inflammation and pyroptosis in AKI rats BMSCs-miR-223-3p-EVs were injected simultaneously with sh-SNRK or sh-NC into AKI rats. **A** miR-223-3p expression measured by qRT-PCR and SNRK mRNA or protein levels determined by qRT-PCR and western blotting in kidney tissues of rats; **B** HE staining, PAS staining, Masson staining, and TUNEL staining to observe histopathological structural changes and apoptosis in the kidney of AKI rats. **C**, **D** Detection of CRE (**C**) and BUN (**D**) level changes. **E** ELISA to examine the levels of proinflammatory factors IL-1β, IL-6, and TNF-α in kidney tissues of AKI rats. **F** Western blotting to evaluate NLRP3, ASC, cleaved caspase-1, and IL-18 expression in kidney tissues of AKI rats. Data were expressed as mean ± standard deviation. $n = 10$ rats/group. $^{*}P < 0.05$ vs. sham-operated rats; $^{\#}P < 0.05$ vs. AKI rats; $^{\&}P < 0.05$ vs. AKI rats treated with BMSCs-miR-223-3p-EVs + sh-NC

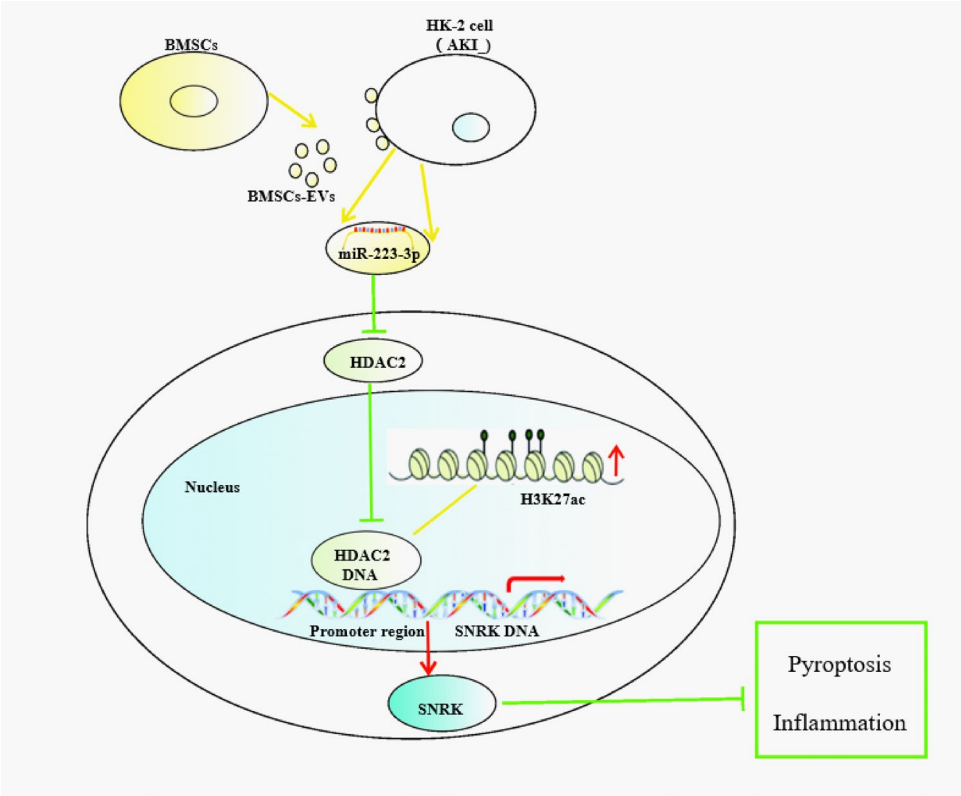

Fig. 8 BMSCs-EV-encapsulated miR-223-3p targets HDAC2 to promote SNRK transcription and attenuate AKI-induced inflammation and pyroptosis. BMSCs secret EVs to carry miR-223-3p that inhibits the expression of deacetylation protein HDAC2 and promotes H3K27ac acetylation, thereby increasing downstream SNRK expression to alleviate AKI-induced inflammation and pyroptosis

EVs could repress endoplasmic reticulum stress and prevent kidney I/R injury by delivering miR-199a-5p [38]. Intriguingly, although Chen et al. noted that BMSC-released EVs overexpressing miR-223 protected against liver injury and inflammation in experimental autoimmune hepatitis [39], little is known about the impacts of BMSC-derived EV-shuttled miR-223-3p on AKI. Nevertheless, the role of miR-223-3p has been researched in AKI. miR-223-3p repression triggered the activation of the NLRP3/caspase-1/IL-1β pathway to promote pyroptosis in renal tubular epithelial cells in septic AKI [40]. Also, another study revealed that miR-223-3p overexpression alleviated inflammation and enhanced viability of LPS-stimulated HK-2 cells by downregulating NLRP3 [41]. Moreover, the findings in our dissertation illustrated that BMSCs-EVs overexpressing miR-223-3p curbed KIM-1 expression, secretion of proinflammatory cytokines, pyroptosis, and apoptosis of LPS-induced HK-2 cells as well as elevated the cell viability. BMSCs-miR-223-3p-EVs also attenuated kidney injury, pyroptosis, and inflammation in AKI rats. These observations contributed to a conclusion that BMSC-derived EVs carrying miR-223-3p ameliorated AKI-triggered pyroptosis and inflammation.

It is widely known that miRNA can reduce the expression of target genes by directing RNA-induced silencing complexes to bind specific target mRNAs to influence numerous biological phenotypes [42]. For example, HDAC2 was a target gene of miR-223 during COVID-19 immunopathogenesis [43]. Similarly, starBase software predicted a targeting relationship between miR-223-3p and HDAC2 in our study, which was validated by dual-luciferase reporter gene and RIP assays. Further rescue experiments established that HDAC2 overexpression nullified the impacts of BMSCs-miR-223-3p-EVs on proinflammatory cytokine secretion, pyroptosis, viability, and apoptosis of LPS-induced HK-2 cells. Importantly, an earlier report found that HDAC2 was upregulated in LPS-stimulated rat renal tubular epithelial cells and that TSA, an HDAC2 inhibitor, lightened sepsis-induced AKI [44]. Besides, the suppressive impact of TSA on AKI was accompanied by decreased inflammation, KIM-1 expression, serum urea, and serum creatinine [45]. Despite no research about the role of HDAC2 in AKI-induced pyroptosis, there was evidence that HDAC2 suppression led to the decline of pyroptosis in acute liver failure and cigarette smoke exposure-stimulated ovarian tissue damage [46, 47].

Interactions between HDACs and DNA contribute to the formation of compacted and inactive chromatin that inhibits gene transcription [48]. In the current research, the UCSC database predicted peak histone H3 acetylation in the SNRK promoter, and further ChIP assay and western blotting exhibited that HDAC2 suppressed H3 acetylation to reduce SNRK transcription. SNRK was observed to exert anti-inflammatory impacts in different diseases. For instance, SNRK is

able to restrain adipocyte inflammation [49]. In addition, SNRK upregulation is noted to subdue cardiac inflammation during heart failure [50]. SNRK repressed inflammation in angiotensin II-induced glomerular endothelial cells by inactivating nuclear factor-κB/p65 [18]. However, there has hitherto been little research about the influence of SNRK on pyroptosis and AKI. Additional rescue experiments in our study manifested that SNRK silencing annulled the effects of BMSCs-miR-223-3p-EVs on inflammation and pyroptosis in LPS-induced HK-2 cells and AKI rats.

Conclusion

Collectively, our findings uncovered that BMSC-derived EVs decreased HDAC2 expression and then enhanced SNRK transcription by delivering miR-223-3p, which alleviated AKI-induced inflammation and pyroptosis (Fig. 8). Investigation of BMSCs-EVs carrying miR-223-3p yields a better understanding for AKI treatment. However, the research is still at the preclinical stage, and the exploration on the mechanism of miR-223-3p in AKI is not yet well elaborated. Interpretation of our results should be cautious, because our data were obtained in rats and cells with experimental AKI which cannot completely mimic the development of AKI in human beings and also because the AKI model was not validated as the source of fulminant sepsis. Hence, similar assays are warranted to further dissect the intrinsic mechanisms.

Acknowledgements Thanks for all the participants and contributors.

Author contributions ZX and QL conceived the ideas; designed the experiments. ZX and JT performed the experiments. ZC analyzed the data. LW provided critical materials. QL and JC wrote the manuscript. QL supervised the study. All the authors have read and approved the final version for publication.

Funding This study was supported by Subject of Hunan Provincial Health Commission in 2022 (202203054143).

Data availability The datasets used or analyzed during the current study are available from the corresponding author on reasonable request.

Declarations

Conflict of interest The authors report no relationships that could be construed as a conflict of interest.

References

1. Levey AS, James MT. Acute kidney injury. Ann Intern Med. 2017. https://doi.org/10.7326/AITC201711070.
2. Ronco C, Bellomo R, Kellum JA. Acute kidney injury. Lancet. 2019;394:1949–64.
3. Farrar A. Acute kidney injury. Nurs Clin North Am. 2018;53:499–510.
4. Kellum JA, Romagnani P, Ashuntantang G, Ronco C, Zarbock A, Anders HJ. Acute kidney injury. Nat Rev Dis Primers. 2021;7:52.
5. Gong L, Pan Q, Yang N. Autophagy and inflammation regulation in acute kidney injury. Front Physiol. 2020;11: 576463.
6. Frank D, Vince JE. Pyroptosis versus necroptosis: similarities, differences, and crosstalk. Cell Death Differ. 2019;26:99–114.
7. Tsuchiya K. Switching from apoptosis to pyroptosis: gasdermin-elicited inflammation and antitumor immunity. Int J Mol Sci. 2021. https://doi.org/10.3390/ijms22010426.
8. Li N, Wang Y, Wang X, Sun N, Gong YH. Pathway network of pyroptosis and its potential inhibitors in acute kidney injury. Pharmacol Res. 2022;175: 106033.
9. Guo J, Wang R, Liu D. Bone marrow-derived mesenchymal stem cells ameliorate sepsis-induced acute kidney injury by promoting mitophagy of renal tubular epithelial cells via the SIRT1/parkin axis. Front Endocrinol (Lausanne). 2021;12: 639165.
10. Abels ER, Breakefield XO. Introduction to extracellular vesicles: biogenesis, rna cargo selection, content, release, and uptake. Cell Mol Neurobiol. 2016;36:301–12.
11. Batsali AK, Georgopoulou A, Mavroudi I, Matheakakis A, Pontikoglou CG, Papadaki HA. The role of bone marrow mesenchymal stem cell derived extracellular vesicles (MSC-EVs) in normal and abnormal hematopoiesis and their therapeutic potential. J Clin Med. 2020. https://doi.org/10.3390/jcm9030856.
12. Zhu G, Pei L, Lin F, Yin H, Li X, He W, et al. Exosomes from human-bone-marrow-derived mesenchymal stem cells protect against renal ischemia/reperfusion injury via transferring miR-199a-3p. J Cell Physiol. 2019;234:23736–49.
13. Ren GL, Zhu J, Li J, Meng XM. Noncoding RNAs in acute kidney injury. J Cell Physiol. 2019;234:2266–76.
14. Tan J, Fan J, He J, Zhao L, Tang H. Knockdown of LncRNA DLX6-AS1 inhibits HK-2 cell pyroptosis via regulating miR-223-3p/NLRP3 pathway in lipopolysaccharide-induced acute kidney injury. J Bioenerg Biomembr. 2020;52:367–76.
15. Lv P, Liu H, Ye T, Yang X, Duan C, Yao X, et al. XIST inhibition attenuates calcium oxalate nephrocalcinosis-induced renal inflammation and oxidative injury via the miR-223/NLRP3 pathway. Oxid Med Cell Longev. 2021;2021:1676152.
16. Ma T, Huang C, Xu Q, Yang Y, Liu Y, Meng X, et al. Suppression of BMP-7 by histone deacetylase 2 promoted apoptosis of renal tubular epithelial cells in acute kidney injury. Cell Death Dis. 2017;8: e3139.
17. Jahan S, Sun JM, He S, Davie JR. Transcription-dependent association of HDAC2 with active chromatin. J Cell Physiol. 2018;233:1650–7.
18. Lu Q, Ma Z, Ding Y, Bedarida T, Chen L, Xie Z, et al. Circulating miR-103a-3p contributes to angiotensin II-induced renal inflammation and fibrosis via a SNRK/NF-kappaB/p65 regulatory axis. Nat Commun. 2019;10:2145.
19. Gong J, Meng HB, Hua J, Song ZS, He ZG, Zhou B, et al. The SDF-1/CXCR4 axis regulates migration of transplanted bone marrow mesenchymal stem cells towards the pancreas in rats with acute pancreatitis. Mol Med Rep. 2014;9:1575–82.
20. Yan W, Wu X, Zhou W, Fong MY, Cao M, Liu J, et al. Cancer-cell-secreted exosomal miR-105 promotes tumour growth through the MYC-dependent metabolic reprogramming of stromal cells. Nat Cell Biol. 2018;20:597–609.
21. Wang H, Mou H, Xu X, Liu C, Zhou G, Gao B. LncRNA KCNQ1OT1 (potassium voltage-gated channel subfamily Q member 1 opposite strand/antisense transcript 1) aggravates acute kidney injury by activating p38/NF-kappaB pathway via miR-212-3p/

MAPK1 (mitogen-activated protein kinase 1) axis in sepsis. Bioengineered. 2021;12:11353–68.
22. Shen Z, Liao X, Shao Z, Feng M, Yuan J, Wang S, et al. Short-term stimulation with histone deacetylase inhibitor trichostatin a induces epithelial-mesenchymal transition in nasopharyngeal carcinoma cells without increasing cell invasion ability. BMC Cancer. 2019;19:262.
23. Soejima M, Koda Y. TaqMan-based real-time PCR for genotyping common polymorphisms of haptoglobin (HP1 and HP2). Clin Chem. 2008;54:1908–13.
24. Bruno S, Grange C, Collino F, Deregibus MC, Cantaluppi V, Biancone L, et al. Microvesicles derived from mesenchymal stem cells enhance survival in a lethal model of acute kidney injury. PLoS ONE. 2012;7: e33115.
25. Reis LA, Borges FT, Simoes MJ, Borges AA, Sinigaglia-Coimbra R, Schor N. Bone marrow-derived mesenchymal stem cells repaired but did not prevent gentamicin-induced acute kidney injury through paracrine effects in rats. PLoS ONE. 2012;7: e44092.
26. Meng F, Chen Q, Gu S, Cui R, Ma Q, Cao R, et al. Inhibition of Circ-Snrk ameliorates apoptosis and inflammation in acute kidney injury by regulating the MAPK pathway. Ren Fail. 2022;44:672–81.
27. Xu HP, Ma XY, Yang C. Circular RNA TLK1 promotes sepsis-associated acute kidney injury by regulating inflammation and oxidative stress through miR-106a-5p/HMGB1 axis. Front Mol Biosci. 2021;8: 660269.
28. Zhang Y, Zhu J, Zhang C, Xiao J, Liu C, Wang S, et al. Non-invasive early prediction of septic acute kidney injury by doppler-based renal resistive indexes combined with echocardiographic parameters: an experimental study. Front Med (Lausanne). 2021;8: 723837.
29. Hoste EAJ, Kellum JA, Selby NM, Zarbock A, Palevsky PM, Bagshaw SM, et al. Global epidemiology and outcomes of acute kidney injury. Nat Rev Nephrol. 2018;14:607–25.
30. Li JK, Yang C, Su Y, Luo JC, Luo MH, Huang DL, et al. Mesenchymal stem cell-derived extracellular vesicles: a potential therapeutic strategy for acute kidney injury. Front Immunol. 2021;12: 684496.
31. Liu P, Feng Y, Wang Y, Zhou Y. Therapeutic action of bone marrow-derived stem cells against acute kidney injury. Life Sci. 2014;115:1–7.
32. Chen Y, Tang X, Li P, Zhou Y, Xue T, Liu J, et al. Bone marrow derived mesenchymal stromal cells ameliorate ischemia/reperfusion injury-induced acute kidney injury in rats via secreting tumor necrosis factor-inducible gene 6 protein. Biomed Res Int. 2019;2019:9845709.
33. Lo Sicco C, Reverberi D, Balbi C, Ulivi V, Principi E, Pascucci L, et al. Mesenchymal stem cell-derived extracellular vesicles as mediators of anti-inflammatory effects: endorsement of macrophage polarization. Stem Cells Transl Med. 2017;6:1018–28.
34. Alzahrani FA. Melatonin improves therapeutic potential of mesenchymal stem cells-derived exosomes against renal ischemia-reperfusion injury in rats. Am J Transl Res. 2019;11:2887–907.
35. Lin Y, Liu M, Chen E, Jiang W, Shi W, Wang Z. Bone marrow-derived mesenchymal stem cells microvesicles stabilize atherosclerotic plaques by inhibiting NLRP3-mediated macrophage pyroptosis. Cell Biol Int. 2021;45:820–30.
36. Schrezenmeier EV, Barasch J, Budde K, Westhoff T, Schmidt-Ott KM. Biomarkers in acute kidney injury—pathophysiological basis and clinical performance. Acta Physiol (Oxf). 2017;219:554–72.
37. Groot M, Lee H. Sorting mechanisms for microRNAs into extracellular vesicles and their associated diseases. Cells. 2020. https://doi.org/10.3390/cells9041044.
38. Wang C, Zhu G, He W, Yin H, Lin F, Gou X, et al. BMSCs protect against renal ischemia-reperfusion injury by secreting exosomes loaded with miR-199a-5p that target BIP to inhibit endoplasmic reticulum stress at the very early reperfusion stages. FASEB J. 2019;33:5440–56.
39. Chen L, Lu FB, Chen DZ, Wu JL, Hu ED, Xu LM, et al. BMSCs-derived miR-223-containing exosomes contribute to liver protection in experimental autoimmune hepatitis. Mol Immunol. 2018;93:38–46.
40. Gao M, Li H, Liu Q, Ma N, Zi P, Shi H, et al. KLF6 promotes pyroptosis of renal tubular epithelial cells in septic acute kidney injury. Shock. 2022;57:417–26.
41. Sun Y, Liu MW, Zhao YH, Lu YX, Wang YA, Tong CW. Baicalin attenuates lipopolysaccharide-induced renal tubular epithelial cell injury by inhibiting the TXNIP/NLRP3 signalling pathway via increasing miR-223-3p expression. J Biol Regul Homeost Agents. 2020;34:69–82.
42. Seok H, Ham J, Jang ES, Chi SW. MicroRNA target recognition: insights from transcriptome-wide non-canonical interactions. Mol Cells. 2016;39:375–81.
43. Houshmandfar S, Saeedi-Boroujeni A, Rashno M, Khodadadi A, Mahmoudian-Sani MR. miRNA-223 as a regulator of inflammation and NLRP3 inflammasome, the main fragments in the puzzle of immunopathogenesis of different inflammatory diseases and COVID-19. Naunyn Schmiedebergs Arch Pharmacol. 2021;394:2187–95.
44. Hsing CH, Lin CF, So E, Sun DP, Chen TC, Li CF, et al. alpha2-Adrenoceptor agonist dexmedetomidine protects septic acute kidney injury through increasing BMP-7 and inhibiting HDAC2 and HDAC5. Am J Physiol Renal Physiol. 2012;303:F1443–53.
45. Jiang W, Yuan X, Zhu H, He C, Ge C, Tang Q, et al. Inhibition of histone H3K27 acetylation orchestrates interleukin-9-mediated and plays an anti-inflammatory role in cisplatin-induced acute kidney injury. Front Immunol. 2020;11:231.
46. Li F, Ding J, Cong Y, Liu B, Miao J, Wu D, et al. Trichostatin A alleviated ovarian tissue damage caused by cigarette smoke exposure. Reprod Toxicol. 2020;93:89–98.
47. Wang Y, Chen Q, Jiao F, Shi C, Pei M, Wang L, et al. Histone deacetylase 2 regulates ULK1 mediated pyroptosis during acute liver failure by the K68 acetylation site. Cell Death Dis. 2021;12:55.
48. Liu YR, Wang JQ, Huang ZG, Chen RN, Cao X, Zhu DC, et al. Histone deacetylase2: a potential regulator and therapeutic target in liver disease (review). Int J Mol Med. 2021. https://doi.org/10.3892/ijmm.2021.4964.
49. Li Y, Nie Y, Helou Y, Ding G, Feng B, Xu G, et al. Identification of sucrose non-fermenting-related kinase (SNRK) as a suppressor of adipocyte inflammation. Diabetes. 2013;62:2396–409.
50. Thirugnanam K, Cossette SM, Lu Q, Chowdhury SR, Harmann LM, Gupta A, et al. Cardiomyocyte-specific snrk prevents inflammation in the heart. J Am Heart Assoc. 2019;8: e012792.